Luís Filipe
Pino Gonçalves

Pipeline de análise de detritos espaciais para o PASO

Space Data Processing Pipeline for PASO

Universidade de Aveiro
2023

Luís Filipe Pino Gonçalves

Pipeline de análise de detritos espaciais para o PASO

Space Data Processing Pipeline for PASO

Dissertação apresentada à Universidade de Aveiro para cumprimento dos requisitos necessários à obtenção do grau de Mestre em Engenharia Física, realizada sob a orientação científica do Doutor Vitor Bonifácio, Professor Auxiliar do Departamento de Física da Universidade de Aveiro e do Doutor Bruno Coelho, investigador do Instituto de Telecomunicações.

o júri / the jury

presidente / president	**Isabel Maria Coelho de Oliveira Malaquias** Associate Professor from Universidade de Aveiro
arguente / examiner	**Dalmiro Jorge Filipe Maia** Researcher from Faculdade de Ciências da Universidade do Porto
orientadores / advisors	**Vitor Hugo da Rosa Bonifácio** Auxiliar Professor from Universidade de Aveiro
	Bruno David Fernandes Coelho Researcher from Instituto de Telecomunicações

acknowledgements

I want to thank both my advisors Dr. Vitor Bonifácio and Dr. Bruno Coelho for their support and teachings throughout the entire process of this thesis. I would also want to thank the entire SST group for the discussions that we had throughout the year and the amazing input that they offered me. A special thanks to Constança Alves for working with me during this thesis, to the PT-MoD for supplying telescope images that allowed me to do this thesis and to T.S. Kelso for providing us with TLEs for specific dates after a simple email contact.

Lastly I would like to thank all my friends and family for their support and encouragement not only through this final chapter of my degree but throughout the entire path, both through the good and difficult times of this journey.

This work is supported by the European Regional Development Fund (FEDER), through the Competitiveness and Internationalization Operational Programme (COMPETE 2020) of the Portugal 2020 framework [Project SmartGlow with Nr. 069733 (POCI-01-0247-FEDER-069733)]; The team acknowledges further support from ENGAGE-SKA Research Infrastructure, ref. POCI-01-0145-FEDER-022217, funded by COMPETE 2020 and FCT, Portugal; IT team members acknowledge support from Projecto Lab. Associado UID/EEA/50008/2019. We acknowledge support by the European Commission H2020 Programme under the grant agreement 2-3SST2018-20.

Palavras-chave

Observatório Espacial da Pampilhosa da Serra (PASO), *Space Surveillance and Tracking* (SST), Pipeline de processamento de dados, satélites; Órbita Média Terrestre (MEO), Órbita Geosíncrona Terrestre (GEO), lixo espacial

Resumo

Os detritos orbitais tornaram-se numa das maiores ameaças para os satélites ativos. Com um aumento nos lançamentos de satélites, o número de pequenos objetos em órbita está aumentando a uma ritmo nunca antes visto. Isto criou a necessidade de rastrear e pesquisar esses objetos no espaço para proteger as missões espaciais presentes e futuras. No âmbito do SST, Portugal está a criar o PASO (PAmpilhosa da Serra Observatory) com a missão principal de monitorizar objetos em todas as órbitas. Já se encontra equipado com um radar capaz de rastrear objetos em LEO e um telescópio óptico capaz de pesquisar e rastrear objetos em MEO e GEO. Nesta tese criámos SPADE, a nova pipeline de dados espaciais que está será usada com o novo sistema de telescópio duplo que está a ser implementado no PASO. Esta pipeline contêm todas as etapas necessárias para analisar uma imagem bruta desde a sua redução, detecção das fontes, astrometria, com possibilidades adicionais de fotometria e identificação dos satélites. O SPADE está atualmente pronto para analisar objetos em MEO e GEO, atingindo a precisão necessária de 2 segundos de arco pelo SST e continuará a ser trabalhado com o objetivo final de analisar objetos em LEO. SPADE foi construído de modo a poder ser utilizado em tempo real sem a criação de filas de processamento de imagens através da utilização de *multi-threading*. O SPADE também foi construído para ser facilmente adaptável a qualquer telescópio e observatório. Cada parte do pipeline pode ser facilmente controlada no arquivo de configuração sem a necessidade de conhecimento profundo do código.

Keywords PAmpilhosa da Serra space Observatory (PASO), Space Surveillance and Tracking (SST), Data Processing Pipeline, satellites, Medium Earth orbit (MEO), Geosynchronous Earth Orbit (GEO), space debris

Abstract Orbital debris have become one of the biggest threats for operational satellites. With an increase in satellite launches the number of small objects in orbit is increasing at a never seen rate. This has created the need to track and survey these objects in order to protect present and future space missions. As part of the SST, Portugal is creating PASO (PAmpilhosa da Serra Observatory) with the main mission of monitoring objects in all orbits. It is already equipped with a radar telescope capable of tracking LEO objects and a optical telescope capable of surveying and tracking MEO and GEO objects. In this thesis we developed SPADE, the new space data pipeline that will be used for the new double telescope system being now implemented in PASO. This pipeline consists of all the steps necessary to analyse a raw image: image reduction, source detection, plate solving with additional possibility of photometry and satellite identification. SPADE is presently ready to analyse MEO and GEO orbits reaching the necessary 2 arcsec precision required by the SST and will continue to be worked on with the final goal of analysing LEO objects. SPADE was built with the goal of providing real-time analysis without the creation of image queues. This was achieved by the usage of multi-threading. SPADE was also built to be easily adaptable to any telescope and observatory. Every part of the pipeline can be easily controlled in the configuration file without the need of in-depth knowledge of the code.

Contents

ADC	Analog-to-Digital Converter
BSI	Back-Side Illuminated
CCD	Charge-Coupled Devices
CMOS	Complementary Metal Oxide Semiconductors
Dec	Declination
EU-SST	EUropean - Space Surveillance and Tracking
FoV	Field of View
FSI	Front-Side Illuminated
FWHM	Full Width Halft Maximum
GEO	Geosynchronous Earth Orbit
GPS	Global Positioning System
GPZ+	GEO Protected Zone Plus
ISS	International Space Station
LEO	Low Earth orbit
MEO	Medium Earth orbit
NoC	National Operation Center
NORAD	North American Aerospace Defense Command
OPD	Observatório Pico dos Dias
PASO	PAmpilhosa da serra Space Observatory
PSF	Point Spread Function
PT-MoD	Portuguese Ministry of Defence
RA	Right Ascension
RAM	Random Access Memory
RSO	Resident Space Objects
SGP4	Simplified General Perturbations 4
SNR	Signal to Noise Ratio
SPADE	SPAce Debris dEtection pipeline
SST	Space Surveillance and Tracking
TLE	Two Line Element
USA	United States of America

Chapter 1

Introduction

Humanity desire for improvement led throughout history to technological development. One interest that was out of grasp was the vastness of outer space, with numerous great minds across time such as Galileu Galilei and Johannes Keppler in the XVII century, but going as far back as the Greeks with Hipparcos and many more. With modern technology, this old dream has finally become a possibility, leading to an enormous boom in space missions during the last century. This effect was increased during the Cold War when the United States of America (USA) and Soviet Union competed for "space domination". As always, there is always a great amount of funding in the military area which led to many feats of engineering such as the first satellite launch (Sputnik) in 1957 or the more known first man on the Moon (Neil Armstrong) in 1969. Every year since Sputnik the number of satellite launches and space missions has been increasing. Today's immense network of satellites gives us access to many tools that have shaped the world, such as the Global Positioning System (GPS) system or the communication sector (Evans, 2010).

Space missions were initially performed with no plan to safely remove satellites from orbit after their mission was complete. This led to the eventual creation of guidelines to safely dispose of satellites after use, with controlled reentries for low orbits, or moved to "graveyard" orbits in the Geosynchronous Earth Orbit (GEO) case. This has been a major success for the GEO orbits, with near-perfect adherence to the guidelines, even though it is not a perfect solution. Increased mission costs led to the guidelines being ignored for more than 80% of the Low Earth orbit (LEO) cases, and the objects were just abandoned to their fate. Even today, a practical solution to remove objects from space has yet to be created after we have lost control. Guidelines need to be more strict in order to preserve valuable orbits for future missions (ESA, 2022).

This has led to a growing accumulation of space debris in orbit as can be seen in figure 1.1, especially in LEO orbits. Even though space is infinite, the volume where we can place orbits is not, which is why this is a problem that has been thought about for a long time, going as far back as 1978 when Donald Kessler predicted that this problem would escalate so much that it would make all orbits unusable. This is now known as the Kessler Syndrome (Kessler & Cour-Palais, 1978). In the next decade, this problem is expected to quickly escalate, like in recent years, as there has been a great number of companies with plans to create mega-constellations of satellites such as SpaceX, OneWeb, and Amazon, with likely others to follow. Another very important problem that appeared in the last few years is the weaponizing of space. Testing of satellite-destroying weapons by various countries like Russia, India, USA and China has resulted in a significant increase in space debris (ESA, 2022; Sheetz, 2022).

In today's world, we can already notice some of the visible consequences caused by the over-population of space, with infamous cases such as the 2009 Iridium-Cosmos collision, various cases of space debris colliding or having very close encounters, with active satellites and even the International Space Station (ISS). This caused damage to the equipment or implied maneuvering the equipment out of way, greatly increasing the cost of operation and decreasing the life expectancy of the mission (Mark Rigby, 2021). With the ever-growing concern that bigger damages may come in the future, there has been a great effort to create solutions that would allow

tracking and survey of space debris in orbit to protect present and future space missions, while there isn't a viable solution to remove these debris from space.

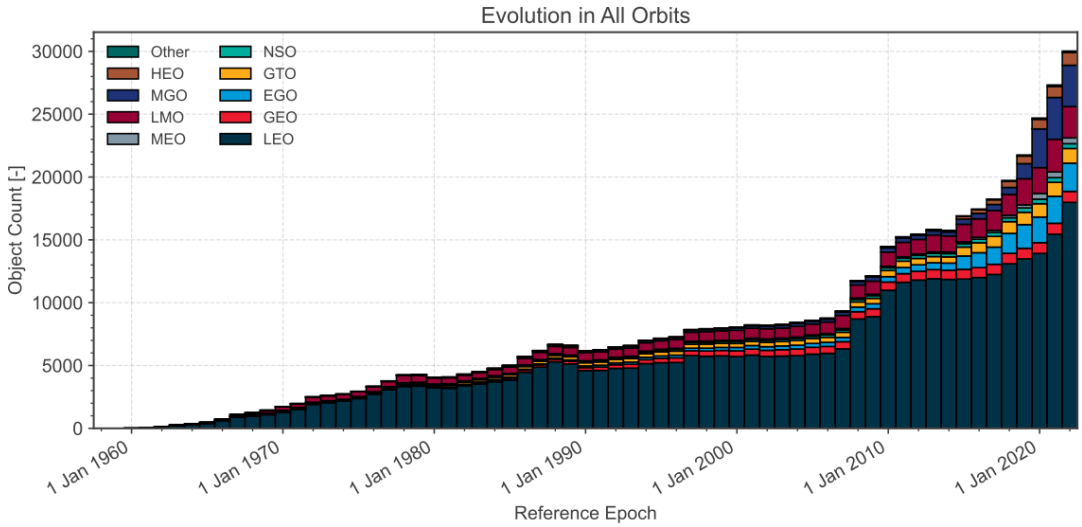

Figure 1.1: Evolution of number of objects in geocentric orbit by orbit class, taken from 2022 ESA's Annual Space Environment Report (ESA, 2022).

As part of this effort the European Union is creating EUropean - Space Surveillance and Tracking (EU-SST)[1], a network of ground-based and space-based sensors capable of surveying and tracking space debris to provide information on space objects in orbit. Within the country's contribution to the consortium, Portugal is creating a new space observatory equipped with both radar and optical telescopes, called PAmpilhosa da serra Space Observatory (PASO), located in the center of the continental Portuguese territory, in the heart of a certified Dark Sky area. There is already one optical telescope installed by the Portuguese Ministry of Defence (PT-MoD) with the main objective of surveying Medium Earth orbit (MEO) and GEO objects as well as monostatic radar focused on LEO tracking. The new double telescope main mission is to be able to survey and track LEO objects in the future, while still be able to operate in the MEO and GEO orbits (Pandeirada et al., 2021).

In terms of ground stations, both types of sensors have their advantages and disadvantages. Radars can observe throughout the entire day, but they can only detect debris on LEO orbits due to their 2000 km range limit. Optical telescopes are best suited for surveillance of high-orbit debris such as MEO or GEO, as there is no issue with range but they can only operate during the night. Consequently in order to properly observe space debris, both sensors types are important because they complement each other. There is an ever-growing interest on utilizing optical systems to complement radar data with other informations such as magnitudes. The main difficulty with this is the need for high-speed mounts and high Field of View (FoV) telescopes, due to the enormous speeds of LEO objects (Virtanen et al., 2016).

In July 2022, a new double optical telescope was installed in PASO with a maximum FoV of $4.3° \times 2.3°$. Its main objective is to track objects in LEO to complement the already installed radar but it can also be used to track and survey objects in MEO and GEO and for scientific research in astronomy. Optical systems are typically used in MEO and GEO but as the demand for objects in LEO has been increasing significantly and is expected to continue for the near future, a solution for this type of orbit needs to be created. The problem is that the LEO regime will be the most challenging to monitor with an optical system due to two difficulties: the fast speed at which the objects cross the sky and the fact that they are only visible right after and before the

[1] https://www.eusst.eu/

sunset, greatly reducing the window of observation. Therefore this set of objects will only start being observed after the system has been thoroughly tested with GEO and MEO objects.

In this work we discuss the current version of SPAce Debris dEtection pipeline (SPADE) which is being developed for the double telescope system in order to create an autonomous solution capable of processing the large amount of data captured every night by the system. The full scheme of the pipeline can be seen in figure 1.2. It can be divided in three main parts: the first being the *Reduction Process* with dark, gain, flat, background, crosstalking and cosmic ray corrections which works to improve our raw data to the best possible conditions, a second part of *Source Detection and characterization* in terms of photometry and astrometry which works to obtain all the information that can be taken from each image, and a third part of *Resident Space Objects (RSO) identification and classification* of satellite/debris from detected sources with the assistance of Two Line Element (TLE)s which works to analyse all the data obtained to reach the final goal of debris detection which will then be given to the costumer. The folder setup of SPADE can be visible in figure A.1.

Given the necessity for these type of solutions, there are a great number of institutions that are working on creating different solutions. One important factor is that there is a great interest in the private sector which means that not all information will be publicly available Added to the fact that there are various methods such as radar or space-based sensors that do not serve for this purpose. Still there is a great amount of literature about RSO detection with innovative methods which gave us ideas on how to tackle the problem. There are a great number of studies about the usage of machine-learning methods such as Jordan et al. (2022, 2023). These methods would require a large data-set of solved images which we do not have, meaning that they could not be immediately used with the new telescope. There are also studies which could be implemented such as Zuehlke et al. (2021) and Sun et al. (2015) which work solely with computer vision methods. The main worry about these studies were the number of false detections that we desperately want to avoid and the time needed as we found those to be quite large to ensure real-time analysis. For these reasons, we decided on attempting to create our own solution. In the future we can attempt to incorporate these different type of solutions, especially machine-learning to see if we can further improve SPADE.

1.1 Double Telescope setup

The new double optical telescope installed in PASO is a wide-field system that can be remotely accessed and controlled. The goal is to develop a completely automatic system, with the assistance of additional equipment such as a meteorological station and a cloud monitoring system to avoid the need of human intervention during observation process (Gonçalves, 2022; Gonçalves L. et al., 2023).

The telescope is equipped with an equatorial mount, that allows the telescope to accompany Earth's rotation and has a maximum slewing speed of 40°, which enables the use for LEO tracking operations, with a 10-arcsecond positioning precision and a 1-arcsecond tracking precision. Each telescope has a $2.3° \times 2.3°$ FoV. The system setup enables two different configurations: the first where both telescopes point at the same area of the sky and two different $2.3° \times 2.3°$ images of the same field are obtained simultaneously, and the second where both telescopes work as one unit with a slight overlap of 0.3° in Declination (Dec) resulting in a total FoV of $4.3° \times 2.3°$, used to maximize the sky survey speed. The cameras installed in the telescopes are SBIG Aluma AC4040 from DIFFRACTION with has a 4096×4096 image resolution and a 9 μm sensor size, resulting in a 2.02 arcsecond/pixel scale. It comes with the possibility of binning 2×2 by hardware, to increase processing speed in SPADE, which would result in a 4.04 arcseconds/pixel scale. The response function of the sensor is known and can be seen in figure 1.4 (left, FSI), having a peak efficiency of 74%. The Complementary Metal Oxide Semiconductors (CMOS) is read at 100 MHz, resulting in a 0.16 seconds read-out time allowing us to take low-exposure images, which is essential for LEO tracking. The minimum exposure time possible is 0.001 seconds, going up to 3600 seconds. With these characteristics, we may use both telescopes to capture videos with more than 10 fps,

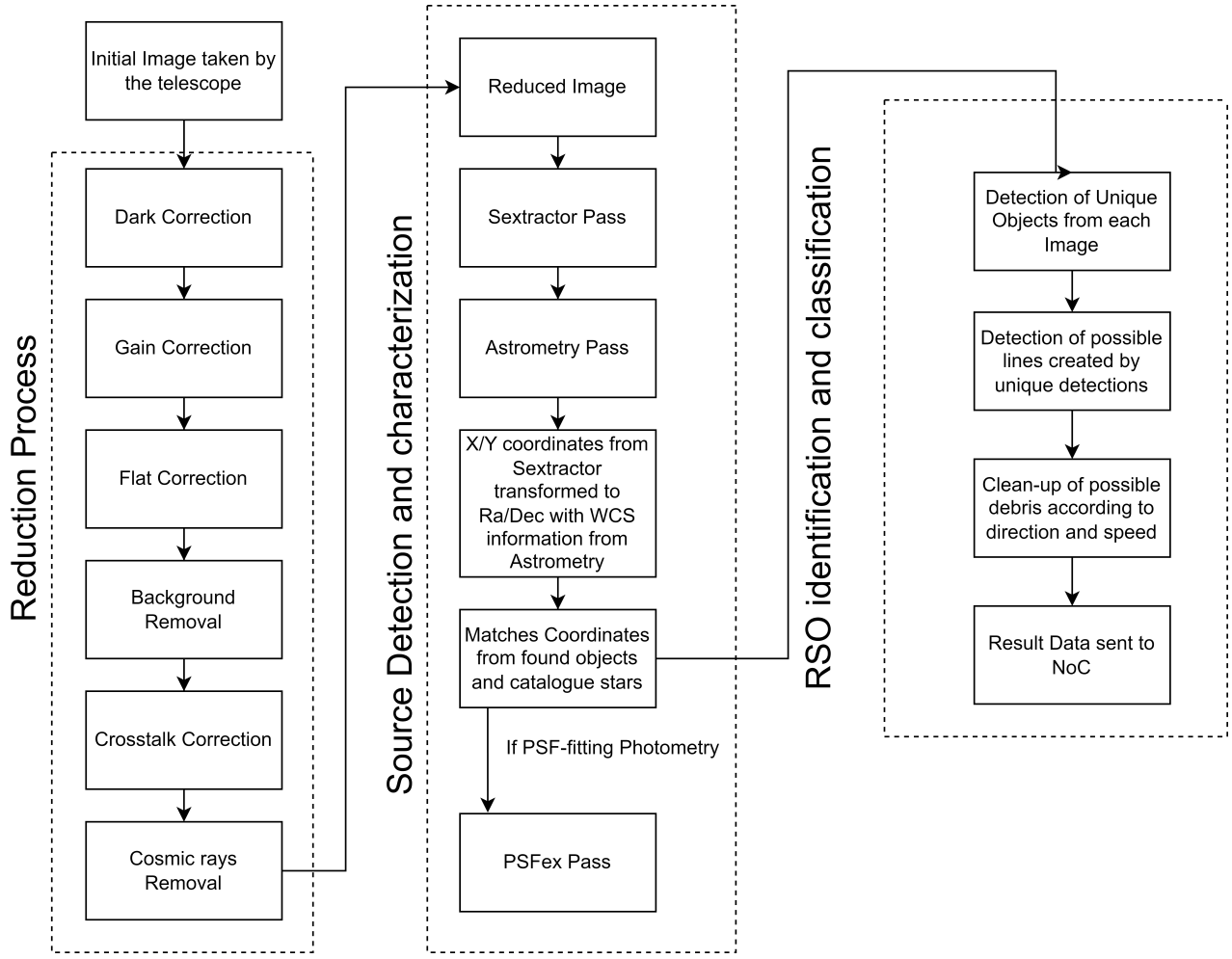

Figure 1.2: SPADE flowchart

allowing us to implement novel solutions such as in Piergentili et al. (2021). The sensor also has the possibility of being cooled to 40° below ambient temperature, with minimal vibration, with a Peltier cooling device to decrease the dark current. Both telescopes also come equipped with a filter wheel with the Johnson-Cousins/Bessel system (BVRI) filters, as well as narrow-band filters, for the [OIII], and Hα lines with the possibility of the usage of [SII] for future work. These will be used to explore the utility of different color filters in the classification and characterization of space debris in the near future. The sensor also comes with an automatic built-in image stacking system to maximize Signal to Noise Ratio (SNR) in our images. The equipment is protected by a clamshell dome, with 3 shutters and a 3 m diameter, capable of opening/closing in 80 seconds. Every component can be controlled remotely.

Initially, the telescope will be used for tracking and surveying satellites and space debris in MEO and GEO orbits, because these possess smaller angular velocities enabling us to better characterize the system. With time and development, the system will then be used for tracking objects in LEO orbits, as that is the final goal. All information about detected debris will be forwarded to National Operation Center (NoC) for further analysis. Due to the amount of data that can be generated in a single night in Space Surveillance and Tracking (SST) usage, the telescope needs a fast, efficient and automatic image-processing software for real-time usage, which will be the purpose for SPADE. In the future there are plans to pair the optical telescopes with the radio telescope, following the example of the MeerLICHT/MeerKAT project used for transient detection, with

information such as debris magnitude (Coelho, 2022; Paterson, 2017).

Figure 1.3: PASO (PAmpilhosa da Serra Observatory) on the left and the new double optical telescope on the right.

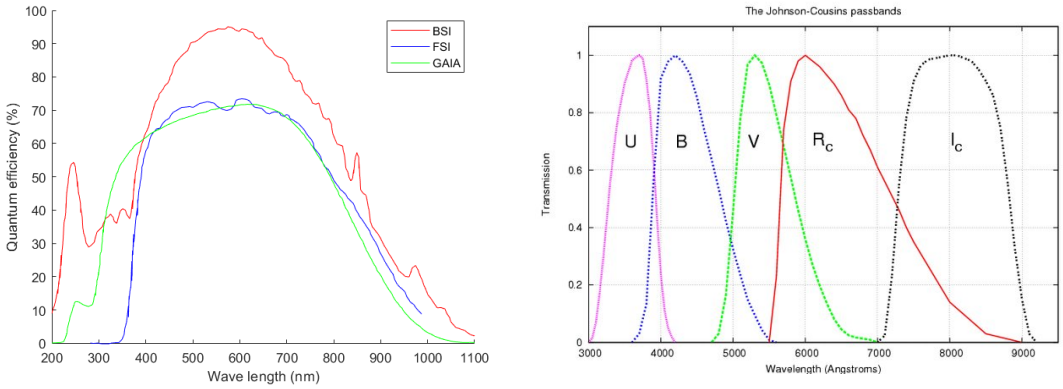

Figure 1.4: Response function for Back Side Illuminated (red), Front Side Illuminated (blue) and GAIA G filter for telescope sensor (green) on the left. Johnson-Cousins filters response functions on the right, image taken from Tawalbeh and Al-Wardat (2018)

1.2 Magnitude System

When we look into the night sky, we can see a large number of stars, with different brightness. The system that is used to characterize the brightness of space objects, the magnitude scale, is one of the oldest scientific standards of measurement, that is still being used today. The system creation dates back all the way to 130 BC, when the Greek astronomer Hipparchus performed his astronomical observations. In order to record the brightness of each object, he established a scale of apparent brightness ranging form 1 (brightest) to 6 (faintest) (Evans, 2010). That explains why the average human observer can only see up to the 6^{th} magnitude with the naked eye. With the development of better telescopes and better technology, astronomers started to observe fainter objects, that would no longer fit in Hipparchus scale. In 1856, Norman Pogson created a fit in order to extend the magnitude scale to higher values, obtaining the logarithm scale that is used nowadays,

$$m - m_{ref} = -2.512\ log_{10}\left(\frac{I}{I_{\text{ref}}}\right). \tag{1.1}$$

The magnitude of an object is a unitless measure, defined in a relative scale to other objects. Each step of magnitude (m) means a change in intensity (I) of about 2.512 in brightness.

There are two main types, the apparent magnitude which relates to how the object appears in the sky and the absolute magnitude which is the magnitude of the object if it where at a fixed

distance from the observer, usually 10 parsec for stars or 1000 km for LEO orbits. The utility of this system is due to the fact that the apparent magnitude of objects can differ significantly due to atmospheric effects or the movement of the object. This does not create a problem for stars, at a first approximation for small FoV, as they are so far away that their light travels approximately through the same atmosphere, so the effect is automatically removed when calibration is performed as all stars suffer the same effect. The main problem comes when observing satellites. Because they are in low orbits, normal approximations can no longer be used since when a satellite/debris moves through the sky, the distance to the observer changes greatly. This effect changes not only the magnitude but also the satellites' illumination. For this reason, one needs to calculate the absolute magnitude in order to compare different observations of objects in order to find if they are the same object.

The next category for magnitudes is the type of filter used for the measurement or bolometric in the case where the entire spectrum is analysed. There is one last point to take into account when talking about magnitudes. With today's technology, we can control which part of the visible spectrum we want to observe with the use of color filters. Every star emits light but not all stars are at the same temperature which means that different stars will have different emission spectrums, resulting in different magnitudes when observed with a filter even though they may have the same bolometric magnitude. There are two main filter systems used in astronomy, the Johnson-Cousins UBVRI system, and the Sloan system. The most usual is the Vegasystem where the star Vega is used to calibrate magnitudes and is considered as having zero magnitude. All other star magnitudes are calculated according to equation 1.1. For comparison, the Sun has an apparent bolometric magnitude of -26.8, while the full moon has a value of -12. The brightest star in the sky (other than the sun) is Sirius with a magnitude of -1.5 (Gasdia, 2016).

In optical images the magnitude that is calculated is designed instrumental magnitude since it is related to the pixel counts and it will change in different sensors. To calibrate the magnitude of optical images catalogue stars are used with the corresponding magnitude. Since the scale is relative, the difference between the two magnitudes will be a number normally called zero-point. To properly calibrate the magnitude of our image we need to make sure we correctly calculate the distance between two points to be sure of our match with the catalogue.

1.3 Angular distance

We need to calculate the distance between two points in order to measure the proximity of two different points. To do this we can't simply calculate the euclidean distance with Right Ascension (RA) and Dec, we need to calculate the angular difference between the two points. The equation 1.2 gives the smallest arc (d) between 2 points on a sphere with coordinates (α_1, δ_1) and (α_2, δ_2). This formula is the exact solution but it becomes computationally hard to calculate when using with very small values of d, or close to 180° (± 10 arcmins). Since we will be calculating distances in the order of arcseconds, there is an alternative solution given by equation 1.3 which allows us to save time in our processing. This approximation is similar to the euclidean distance but with a correction due to the fact that the length of the RA circles will depend on the Dec value. Both options are available in SPADE, with the choice given to the user, with the approximation being the default.

$$d = \cos^{-1}(\sin(\delta_1)\sin(\delta_2) + \cos(\delta_1)\cos(\delta_2)\cos(\alpha_1 - \alpha_2)) \tag{1.2}$$

$$d = \sqrt{\cos^2(\delta_1) \times \Delta\alpha^2 + \Delta\delta^2} \tag{1.3}$$

This equation is derived with a geocentric view which is not a problem for stars as their distance to Earth is significantly bigger than Earth radius and so it is possible to neglect this factor. This is no longer the case when we apply to artificial satellites, especially in LEO orbits, since the Earth radius (≈6400km) is bigger than the altitude of the orbit (<2000km). For GEO and MEO orbits

this effect is much smaller which makes it applicable but still originates some error that needs to be taken into account

1.4 TLE orbit prediction model

An orbital prediction model for satellite positions is a necessary tool to keep up with all debris already observed in space. There are a multitude of methods to predict the orbit of objects in space, each with its own advantages and disadvantages. Today's most common model for satellites or space debris is the North American Aerospace Defense Command (NORAD)'s Simplified General Perturbations 4 (SGP4) which uses TLEs created from telescope observations, not depending on satellite sensors data. This allows it to be used for deactivated satellites.

This technique has been in use for decades proving how valuable it is as a tool. But like everything it has limitations that need to be understood to correctly use them. The SGP4 model created in the 1960s had to cope with severe limitations on both software and hardware components, when compared with today's technology. To compensate for this the method was made quite simple with several effects ignored which are present in more recent methods. This simplicity originates very important limitations for TLEs that may even render them useless for some applications such as the fact that they do not have into account manoeuvres and it does not originate a covariance matrix which makes them hard to use for conjunction operations which is the main concern for SST missions. Due to how long and how much it has been in use there are already been made intensive tests to determine the reliability of TLE predictions, reaching a general conclusion that it only lasts a few days. This requires a continuous operation to keep an active debris catalogue with a risk of loss when manoeuvres occur that greatly change the orbit (Vallado & Cefola, 2012).

In SPADE we do not create our own TLEs as that data processing part is done posteriorly. To obtain the most up-to-date TLEs possible, SPADE daily downloads the available information from CelesTrak[2], a website that works to maintain a public TLE catalogue. To then propagate the orbit and make predictions for the time of our images, SPADE uses the package SkyField, the standard for the astronomical community that allows us to generate high-precision research-grade positions for Earth satellites (Rhodes, 2019). To test SPADE other tools were also used as references such as GPredict and Stellarium. To confirm our results, we compared our predictions, with the same TLE, with the result given in both software and observed an almost perfect match.

1.5 Available Data

We tested SPADE with three different data-set of images. The first one was taken in the Observatório Pico dos Dias (OPD) and is comprised by 20 images from an old mission of scientific research. These images have a small FoV and a large magnitude depth. Even though these are quite different from the images that we expect to obtain, this set comes with flat and dark frames meaning they could be used to test the reduction process. All information about this data-set of files can be seen in table 1.1. The second data-set was provided by PT-MoD and is composed by 60 images from survey operations obtained with the deployable telescope currently installed in PASO. These images are very similar to the ones we will be processing in the future and are grouped in sets of 4 which allowed us to better develop the RSO detection part. These do not come with any set of dark or flat frames. All information about this set of files can be seen in table 1.2. There is an additional data-set provided by the PT-MoD 26 images taken at RA = 12h25m20.00s and Dec = 12°25m20.00s. These are neither at an area of the sky of interest nor it is the expected strategy that will be used but they could be used to test the initial steps until the debris classification process begins.

There are some effects that are present in the PT-MoD data-set that need to be discussed. These effects will cause some difficulties for SPADE and compromise our results. The advantage is

[2]https://celestrak.org/NORAD/elements/

Table 1.1: Number of files from the data-set provided by OPD, per exposure time and color filters. These images were taken beginning at 22:31:46 of 28/05/2014 at Lat=-22.534831° and Long=-45.58302°.

Image Type	Filters	Exposure time (s)						
		20	30	60	65	100	105	240
Dark	-	10		10		10		
Flat	B		30					
	R		30					
Image	B				5			6
	R	4					4	

Table 1.2: Available files from the data-set provided by the PT-MoD and respective coordinates of the observed fields taken beginning at 19:59:56 UTC of 28/02/2023 at Lat=40.182416° and Long=-7.874175°. All images have an exposure time of 1.2s and are taken with 5 seconds intervals.

Field	1	2	3	4	5	6	7	8	9
Ra (h:m:s)	08:07:00	08:07:00	04:23:47	04:23:47	04:23:47	04:23:47	04:23:47	08:07:00	08:07:00
Dec (d:m:s)	-05:11:42	02:24:52	-3:13:45	06:55:00	00:41:33	01:50:37	-08:18:07	-07:43:53	04:57:03
Sets	1	2	3,5	4,6,8,10	7,9	11,13	12	14	15

that these images already serve as a case study for SPADE to be able to work around if it happens in our future images.

The biggest problem is that all images provided by the PT-MoD are unfocused and badly collimated. These problems make it so that stars do not appear as points sources but as "donuts" shaped in the center of the image and "beans" shaped on the top corners, deteriorating the Point Spread Function (PSF) of all sources in the image. These problems are visible in figure 1.5.

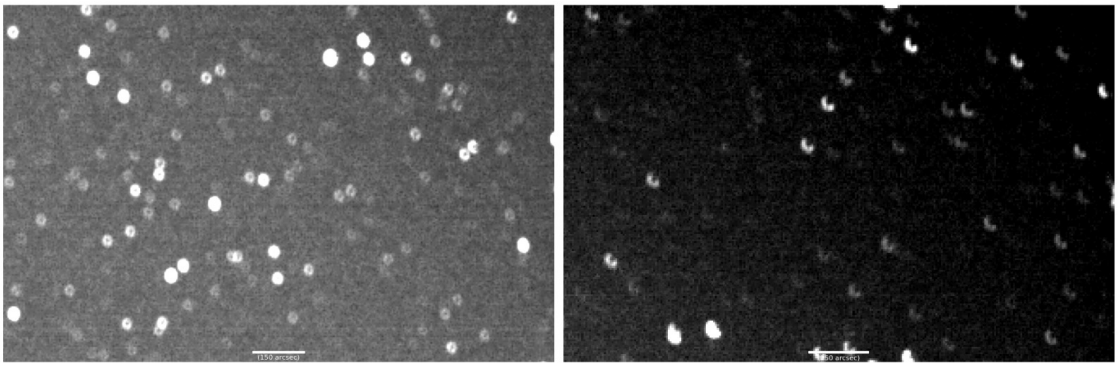

Figure 1.5: Zoom of two areas from set 1 of the images from data-set 2 given by the PT-MoD where the bad quality in the focus is visible (left) and where the non-alignment of collimation of the system (right). The scale is provided by the small while line which corresponds to 150 arcsec.

The second problem that is also due to operation is the start of exposure before the telescope stops stretching all sources in the first image of the set. This deteriorates the quality of the astrometry as will be seen in section 3.2. This effect is shown in figure 1.6. We need to take these effects into account when analysing the results provided by SPADE. We expect not to make the same mistake when we obtain our own images in the future.

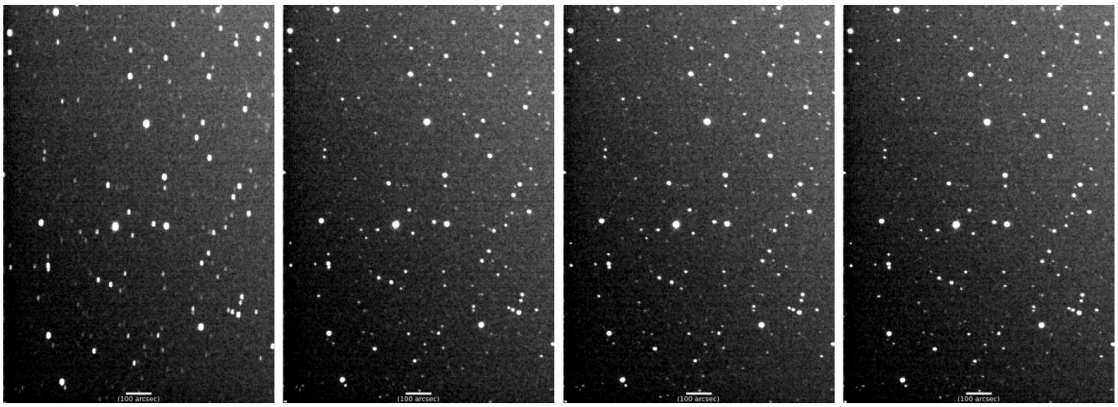

Figure 1.6: Zoom of the same area from all images of set 15 from the data-set given by the PT-MoD where the slight elongation of sources is visible in the first image when compared with the remaining images of the same set. The scale is provided by the small while line which corresponds to 100 arcsec.

Seeing that for SST usage the telescope can be operating in less than ideal conditions, some disturbance such as high speed wind can affect the quality of the image. We have already tackled this problem in the setup of our double telescope as the dome foundation is separated from the telescopes' which will greatly minimize this effect. This isn't the case for the PT-MoD system which will result in less resistance to windy conditions. In the data-set provided this can be seen in one image showcased in figure 1.7 (left). Strong winds will shake the sensor which will give the impression of duplicate sources. Seeing that every source will duplicate the number of detected sources will greatly increase when compared with the rest of the set. For this reason, we can immediately remove the damaged image.

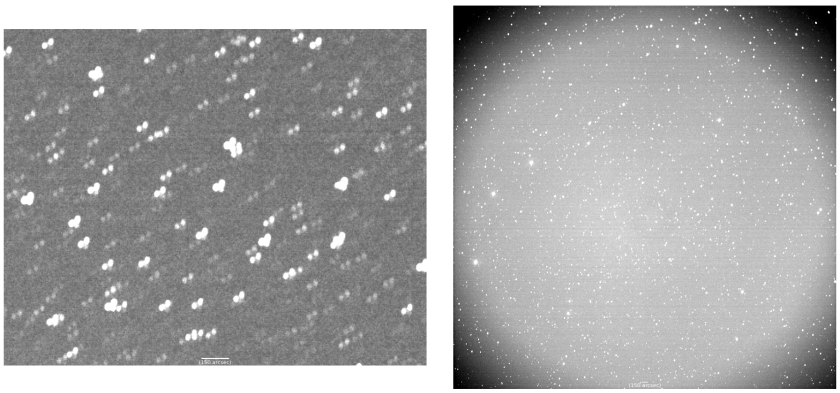

Figure 1.7: Examples of two reduced images from the data-set given by the PT-MoD. On the left image we can see the case where turbulence originated duplicated sources in the image and on the right case we can see the increase in the background brightness due to outside illumination. The scale is provided by the small while line in each image which corresponds to 150 arcsec.

One important factor is the position of the moon during these nights especially when a very large number of fields are observed such as our case. In figure 1.8 we can observe the night sky for the beginning of the exposures. We can immediately see that the moon was visible with coordinates of RA = 5h44m46.87s and Dec = $27°08'52.6''$ meaning that it can have an effect in

our images. In figure 1.7 (right) we can see the effect on some of our images, where the background is much brighter than usual. This will decrease the number of detections that we can detect with the same threshold. It will also worsen the problem originated by the vignetting of the optical system already visible in our images. With the usage of flats this problem should decrease but that test can not be performed with the current data-set as there are no flats available.

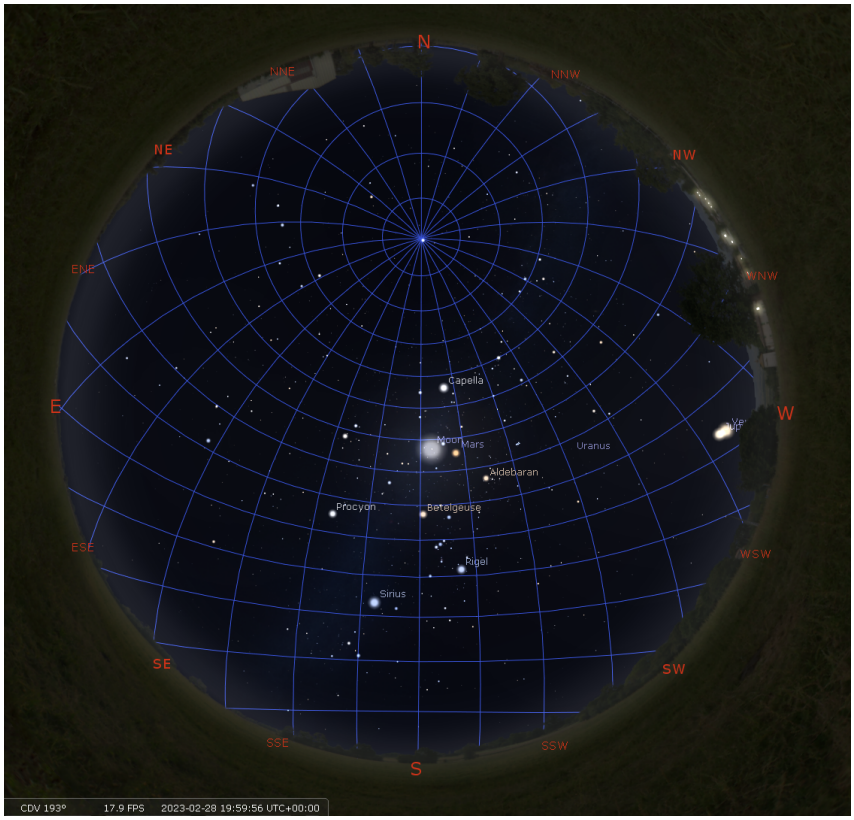

Figure 1.8: Stellarium's Night sky at 19:59:56 UTC of 28/02/2023 at Lat=40.182416° and Long=-7.874175°. The celestial grid is superimposed in the image. The celestial North pole is visible and consecutive RA and Dec lines are 10° apart. We can immediately observe that the moon was visible during that night illuminated 64.4%.

1.6 Catalog Choice

We analyzed four catalogues: Hipparcos, Tycho2, UCAC5, and GAIA. The biggest difference between these catalogues is their number of stars. Hipparcos contains around 118000 objects up to magnitude 11 (Perryman et al., 1997). Comparatively, Tycho-2 is the continuation of the Hipparcos mission and contains the 2.5 million brightest objects. It is much more complete compared to Hipparcos reaching 99 % completeness up to magnitude 11 (V) and 90 % up to magnitude 11.5 (V) (Høg et al., 2000). The UCAC5, created by the U.S. Naval Observatory, also contains the stars from the previous catalogues and adds more to reach more than 100 million objects to magnitudes 16. Lastly, there is the GAIA catalogue. It has information on over 1 billion objects and is currently the most complete catalogue, reaching magnitudes as big as 21 (Gavras et al., 2022).

Even though a catalogue with more objects and a higher magnitude level decreases the number of false negatives and enables us to analyze deeper images, it also comes with the downside of an increase in file size. For instance, the Hipparcos and Tycho-2 catalogues sizes are in the MB

range, around 5 and 500 respectively. The UCAC4 increases to about 6GB in space and the GAIA reaches about 10 TB! This originates a big strain on the hardware of the observatory needed to store bigger data and significantly slows down the processing speed of algorithms, as it needs to check a larger number of stars.

Initially, the Hipparcos and the GAIA catalogues were immediately discarded as the Hipparcos had too few stars for the intended purpose and the GAIA catalog was too big for usage with our current capabilities. Further analysis was only done on the Tycho-2 and the UCAC4 catalogues.

The size of the Tycho-2 catalogue enables it to be easily stored in memory, not creating a big strain on the hardware. This is not the case for the UCAC4 catalogue, as it would consume too big a portion of our Random Access Memory (RAM) possibly requiring the upgrade of the equipment. This effect can be minimized by only reading a portion of the catalogue, either the portion of the sky of interest to the image or the portion of interest for the specific night. However, the UCAC4 catalogue would decrease the number of false negatives and would allow SPADE to be used for deeper images.

To analyze which would be the best choice for the pipeline, we tested with data-sets 2 and 3 given by the PT-MoD. In table 1.4 we can see the percentage of detections that were found in the catalogue for the Hipparcos, Tycho2 and UCAC5 catalogs. The test wasn't performed for the GAIA catalogue due to the fact that it was removed since it was too big for implementation. As we can see, only the UCAC5 reaches a percentage of matching sufficient for implementation. This was expected seeing that Hipparcos and Tycho2 have a small number of sources, not being suitable for the levels of magnitudes that we desire.

Table 1.3: Catalogues and their properties, number of objects, completed magnitude, file size, available filters and astronomical precision.

Catalog	N° objects	$Mag_{completed}$	Size	Filters	Precision (Ra,Dec)
Hipparcos	118k	9	4.7 MB	V	0.77/0.64 mas
Tycho2	2.5M	11	528 MB	BT,VT	7 mas
UCAC5	107M	16	6.5 GB	G,U,R,J,H,K	8-60 mas
GAIA	1.46B	21	10 TB	G,G_{BP},G_{RP}	μas

Table 1.4: Average percentage of matches for detections with a 5σ threshold, a Full Width Halft Maximum (FWHM) threshold for maximum separation and a maximum magnitude of 16 for each tested catalog.

Catalogue	Percentage of Matches
Hipparcos	2.5%
Tycho2	21.1%
UCAC5	97.6%

A decision needed to be done for the maximum value allowed for the separation between our calculated coordinates and the ones given in the catalogue. This value needs to be chosen according to the biggest error that we have in our values. Since the catalogue has very good astrometric precision, the limiting factor is given by our image. We decided on using the median FWHM of all detections in the image as our criteria for the maximum distance. The median was chosen, instead of the mean, due to the fact that some extreme values of FWHM may occur due to some wrong detections. In these cases the mean is greatly affected while the median has a reduced effect, protecting our comparison from outliers. This thought process was the same for all cross-references in SPADE which will occur later.

There is one last point that needs to be taken into account in SPADE which is the epoch of the information. This is because star coordinates change in the celestial coordinate system. Two effects cause this: the first dominant factor is due to Earth's procession, which has a period of around 26000 years and the second much smaller due to the motion of stars in relation to Earth. The first factor will affect the position of the equinox which is used as the origin of the RA axis.

This means that this will originate a movement of around 50 arcsec/year for every object. For this reason and to more easily compare information taken in different years, the astronomical community decided on a common date to save the coordinates of the stars. It was decided that the catalogues would be updated every 50 years starting in 1900. This means that today, in 2023, we use the J2000 epoch for catalogue coordinates. The second and much smaller factor is due to the proper motion of the star, the motion of the star in relation to Earth which is most dominant for objects closer to us. There are stars that have very big values of proper motion such as the Barnard Star which has the biggest value at 10.3 arcsec/year. For most cases though this value is much smaller, in the mas range. This effect could become important if a significant amount of time passed between the measurements taken. To have an understanding, an error of 1 arcsec after 23 years requires a proper motion of 43.5 miliarsec/year. For it to extend to a pixel it would increase to 200 miliarcsec/year. At a first glance, this might seem a problem that needs to be corrected but by analysing the UCAC5 catalogue we discover that these cases happen for only 2.5% and 0.02% respectively. These percentages are so small that they aren't statistically significant in the entire field.

Chapter 2

Data Reduction

Before analysing the image to detect RSOs, corrections may be applied to correct for instrumental effects. This correction process is widely called reduction in astronomy. In this chapter, we will discuss some effects that are present and how they are corrected in SPADE.

2.1 CMOS Detector Principle

One of the most important parts of an optical system is the detector. The way that the telescope captures photons and transforms them into a digital form varies from detector to detector and may cause specific defects that need to be corrected.

There are two main types of detectors used in telescopes: the older and more established Charge-Coupled Devices (CCD) and the CMOS. They have more similarities than not, both being made from silicon chips which will result in similar response functions. In both cases they are composed of an array of photo-active capacitors that accumulate charge due to electron excitation from photons that hit each pixel. The main difference between the two comes in how the information is read. On the CCD when the exposure is complete the charge is transferred from row to row until it reaches the bottom and is read as a serial register. The signal is then fed into an amplifier before it passes through an Analog-to-Digital Converter (ADC) for the final value that we see in the image file. On the CMOS this process occurs in each individual pixel (Gasdia, 2016; Patterson, 2018). This small difference causes the CMOS to have considerably faster reading times while still requiring less power when compared to the CCD. Because of this massive advantage, CMOS are widely chosen for many mobile applications such as phones or webcams where battery life and equipment size is critical. Consequently CMOS have been widely studied in the last decades which in turn has has driven the production price down and created improvements in comparison with the CCD. CMOS disadvantages are that due to the extra circuitry present in each pixel the fill factor, the percentage of the light-sensitive area on each pixel is reduced, reducing the overall photons collected and the sensitivity. This effect is now corrected with small microlenses above each pixel that focus all light that would hit the non-light-sensitive area onto the active region. Still, it is not a perfect solution and the CCD sensor usually has a bigger SNR than the CMOS (Gasdia, 2016; Patterson, 2018).

One of the biggest contributors to CMOS losses is the electronics present in each pixel. These electronic layers can cause the light to be scattered or even absorbed, reducing the amount of light that actually reaches the active area. This problem divides the CMOS into two main types, depending on how the light reaches the sensor: Back-Side Illuminated (BSI) and Front-Side Illuminated (FSI) sensors. The more common type of CMOS sensor is the FSI type which has the electronics between the lens and the photoactive area, an easier option that reduces costs but it means that not all photons can be absorbed by the sensor. With innovation in technology and to increase sensor efficiency, the electronics layer can now be placed behind the photoactive area (BSI). This position eliminates the problem created by the absorption of this layer but the caveat

is that it increases the dark current produced which increases the overall noise of the sensor. Dark current is created because any object above 0K emits radiation that leads to some electrons being excited and originate counts in our detector even if no photons are actually hitting the photoactive area. Overall, the BSI sensors capture more photons, which ultimately results in better images even taking into consideration the noise. The main disadvantage is that due to this technology novelty, the increase in price is significant which can be detrimental for certain projects (Gasdia, 2016; Patterson, 2018). For this reason, we chose the FSI for the PASO double telescope as the advantages did not compensate enough.

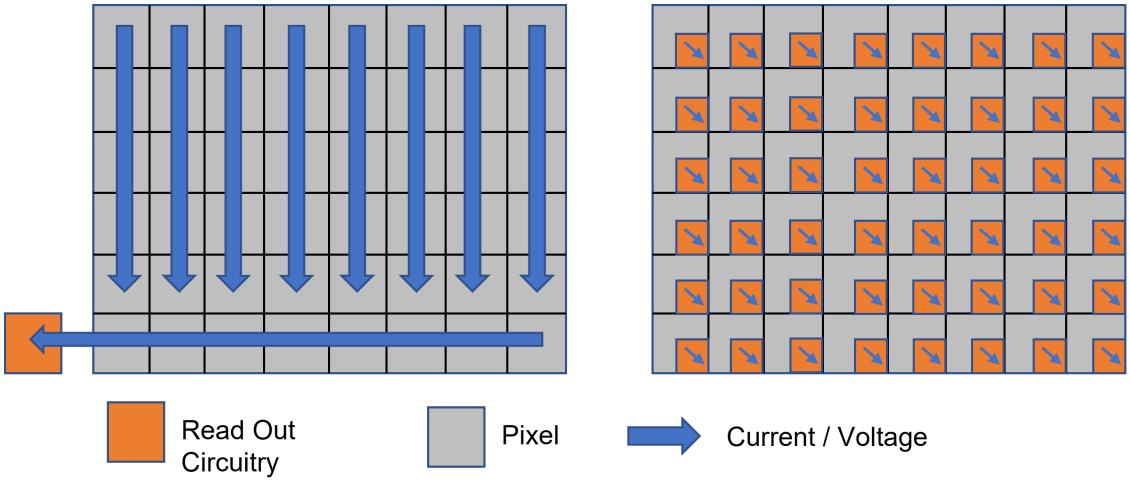

Figure 2.1: Illustration of the difference in the circuitry between the CCD (left) and the CMOS (right). Image adapted from Vision and Robotics (2020).

2.2 Data Reduction

The reduction applied in the SPADE pipeline consists of the following steps: dark frame, flat field, crosstalk, gain, cosmic rays, and background correction. Each step is independent and can be enabled/disabled easily for personal use, visually displayed in figure 1.2.

2.2.1 Dark

The first step of the reduction process is dark field correction. This current will accumulate charge throughout the exposure which will create an offset from the real value. The radiation spectrum emitted by an object depends on its temperature, so this effect can be minimized by cooling the cameras. The main difficulty in this correction is that dark current accumulates at different rates for different pixels, usually called “hot” and “cold” for the ones that accumulate more or less respectively. To correct this effect, an image with the same exposure time as our image is taken with the shutter closed, removing electron excitation due to external sources. This is called a dark frame. Since every pixel is consistent with the dark current that it produces for a given temperature, we can subtract the dark frame from our image to remove the fixed pattern created. Unfortunately, this accumulation of charge is a random process so the effect can never be fully removed and this correction can even add more noise. To minimize the addition of noise to our data, a few dark frames are taken for each exposure time and a master frame is created with the median of all dark frames. This will decrease the noise originating from this process by a factor of 2 every time we quadruple the number of dark frames (Gasdia, 2016; Patterson, 2018). An example of a master dark from our images can be seen in figure 2.2 (left). Master darks are applied both to images and flats, always chosen the one with the closest exposure time and always shorter.

2.2.2 Flat Field

The second step is the flat-field correction. Since not all pixels are built equally, not all pixels will have the same sensitivity. Adding to this, they will also not be illuminated in the same way due to vignetting of the optical system. This will create a difference in counts between different pixels even in cases where they are observing objects with the same light intensity. To correct this effect, an image is taken by illuminating the sensor with an uniform light. This is called a flat frame. This is done either by pointing the telescope to an area of the sky with uniform light, normally in twilight conditions to avoid stars, or by illuminating a white screen inside the dome with a bright light. The advantage of the last method is that it does not depend on natural effects so it is more reliable, the disadvantage is that it requires the installation of additional equipment. The flat frame exposure time is chosen to obtain the maximum possible SNR value while the sensor has a linear response. This frame is also corrected for dark current. This effect varies for different color filters. For this reason one flat frame needs to be taken for each color filter. For the same reason as the master dark, a master flat is created by taking the median of multiple flat frames and in this case the final pixel values are normalized with respect to the maximum (Gasdia, 2016; Patterson, 2018). Each image is then divided by the master flat to perform the correction. An example of a master flat can be seen in figure 2.2 (right).

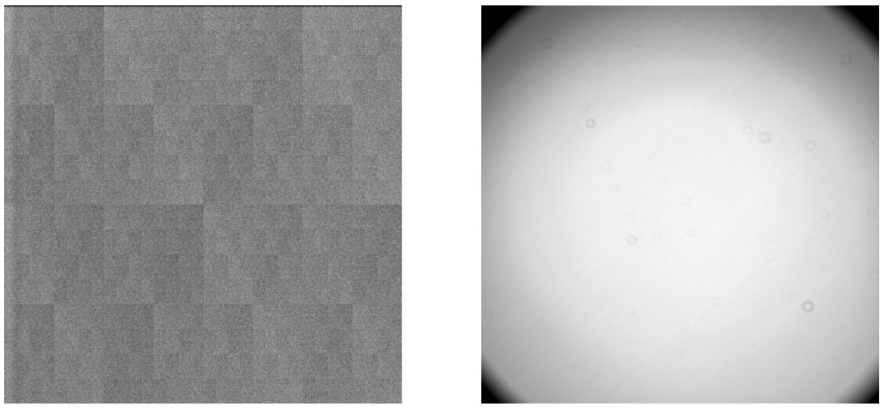

Figure 2.2: Master files examples, Dark on the left and Flat on the right. The vignetting effect is clear in the flat frame and the presence of patterns created by dark current in the dark frame.

2.2.3 Crosstalk

The third step is crosstalk correction. Due to non-perfect insulation between pixels, electrical interference between neighbouring pixels occurs, especially in high-contrast zones. This results in charge being transferred, changing the final readout count in each pixel. This happens with stars in astronomical images. According to McCullough (2008), this effect can be corrected by using a convolution filter to produce the opposite effect. Even though this effect is not critical for general use cases, but in applications where extremely high precision is required, this option is implemented and can be enabled to improve results.

2.2.4 Cosmic Rays

The fourth correction applied to our images is cosmic rays removal. Due to the high energy of a cosmic ray, when it hits a pixel in the detector it will excite a large number of electrons in our sensor, leading to high counts in the output image. Depending on the angle that the cosmic

ray hits the sensor, it can create high counts on a single pixel (perpendicular) or a line of pixels (diagonal), so it becomes a bigger problem than removing isolated pixels. Because we want to detect space debris in orbit, we will need to analyse slightly stretched sources which should not be present. The appearance of cosmic rays in our image may create a false positive in our image analysis algorithm that we want to avoid. To do this, we first need to remove all possible cosmic rays. Objects in our image will have a known PSF whereas cosmic rays will have only a peak in a pixel or set of pixels. By analyzing the shape of these peaks, we can understand whether it is a point source or a cosmic ray. To do this step, SPADE uses "astroscrappy", a python library already build for this purpose (McCully et al., 2018).

2.2.5 Background

The fifth correction is background removal. Like in most applications, there is an amount of signal that is due to effects not important to the case study. In this case, an immense number of objects in space may not be strong enough to be visible with our detector but some of their photons will eventually reach it. The sum of all these sources will create a background signal in our image not due to the point source that we are viewing. This background level is not constant in the entire sky, so a close analysis needs to be performed. This can be removed by analysing the entire image as the background pixels should greatly outnumber the stars. This is a good solution for small FoV but not a good approximation for bigger FoV like ours due to significant variations across the image. To solve that issue, in SPADE the image is divided into multiple subregions to work both in cases where the background is generally consistent in the entire image as well as cases where the background may differ throughout the image. This low-resolution map is then resized to fit the full image. This step is done with the help of "photutils", a python library.

2.2.6 Gain

The last step is gain correction which corrects the counts according to the gain used for the image. This correction is optional and is useful to compare different images of the same field that have been taken with different gain levels. This can occur when comparing images of the same field taken in different days or with images taken from different telescopes which can happen in the double telescope setup in PASO.

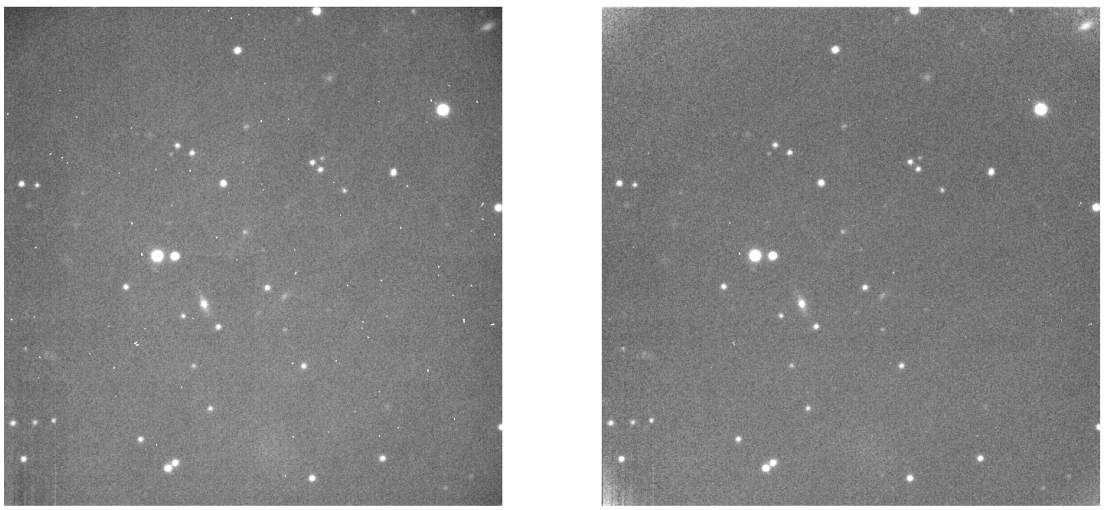

Figure 2.3: Original (left) and corrected (right) images. The disappearance of the dark current patterns, and the correction of vignetting are easily noticeable.

2.3 Time Analysis

A very important step in a real-time processing algorithm is the speed at which it can operate so we can know what are the its limits and if we can push further. In this section we will study how much time is required for each step in the reduction process and the effect of incorporating multi-threading. These values can help us decide which steps should be removed or improved first if SPADE needs to operate faster. We used the available data-sets for this analysis and the time results can be seen in table 2.1 for data-set 1 and table 2.2 for the data-sets 2 and 3. Calculations were performed in a virtual machine created on my personal computer with 10GB of RAM and 8 cores with a AMD Ryzen 5 4600H with Radeon Graphics 3.00 GHz processor.

The first thing that jumps out when we look at these tables is the clear domination of the cosmic ray removal step in the time taken for the reduction process. It surpasses by almost 10× the second slowest step which is background removal. This makes it seem that this should be the first step to be considered for removal in case that SPADE needs to be sped up. The problem is that this might be the most important step to prevent false positives in our final results which is vital. For that reason a careful balance should be done before this step is removed. Another factor to notice is that the Gain, Background and Crosstalk correction times are similar in both data-sets. This is expected as both data-sets have images with the same 2048×2048 resolution and 2 bytes per pixel. The same can not be said for the Cosmic Ray correction which is visibly slower in the second data-set. This can be explained by the fact that the second data-set is composed by images with a significantly higher number of detections which slows down this step. This is a sign that denser fields will originate problems to the cosmic ray correction but not on the other steps.

Looking at the multi-threading factor we notice that as we increase the number of threads available to SPADE we see an increase in the time taken for each individual images. This is expected as the computer needs to divide its resources across all threads. But the overall time taken for the entire data-set decreases as we increase the number of threads. According to Subramaniam (2011) the number of optimal threads depends on the type of problem. In the case where all tasks are computationally intensive like in the case of SPADE, the optimal number of threads will be the number of cores available to the machine.

On the first data-set we can see that this does not hold given that we have 8 cores in the machine and the best case is the 4 threads option. This can be explained due to the fact that we only have 20 images in the data-set, which will mean that with 8 threads 8 images will be processed, then another 8, and then only 4 will be left for the 8 threads. This leaves 4 out of 8 useless in the final part. This does not happen for the 4 threads case as all threads are always used. Given that we do not have additional images of this data-set we can not test this theory. But we can look at the results from data-set of images given by the PT-MoD which has more images. In this data-set the 8 threads produces the best results. This supports the expected that in usual cases this is the best option. But this also creates another question. How many images do we expect to be in queue to be analysed at a given time? The answer to that question may influence the number of threads chosen for SPADE. If we don't expect to have a sufficient number of images to occupy all threads, then lower threads options that match the number of expected images may end up being faster. This discussion will be further looked into in section 3.6.7.

The third important aspect we can take from table 2.1 is the time taken for the dark and flat field corrections. As we can see, these corrections take less time than the cosmic ray removal by a factor of 100. For this reason we can assume that these steps do not slow down the pipeline a considerable amount. The PT-MoD does not currently utilize flat field or dark corrections. Seeing that the time taken for these corrections is small in comparison with the rest, the only setback is on the preparation of the master files required, taking into account both the time taken to actually acquire the dark and flat frames and the time to create the masters. In fact, this also does not pose a problem as it can be done prior to the sky conditions required for the telescope observation as dark frames are obtained with the telescope shut and the flat frames may be acquired before or after the night observation. To make sure, we analysed the time taken to create the master files. We discovered that this process required 29.83 seconds for 5 master files, around 6 seconds per master file. This value does not really pose a problem to the normal operation of the telescope

as it can easily be done prior to the start. The only problem that may arise is needing someone to take these prior to the observations but the process can be automatized. For these reasons, we will be using flat and dark field corrections to improve results.

Table 2.1: Average time in seconds for each step in the reduction process for the set of 20 images from OPD for different number of threads used in multi-threading. Table also presents the total time required by SPADE to process the entire set of images. Calculations were performed in a virtual machine with 10GB of RAM and 8 cores.

Reduction Process	Average Time per Image (s)				
Number of Threads	1	2	4	8	10
Dark Field	0.044	0.058	0.107	0.262	0.360
Flat Field	0.078	0.087	0.163	0.440	0.481
Gain	0.005	0.007	0.012	0.036	0.039
Background	0.513	0.586	0.997	1.983	2.612
Crosstalk	0.017	0.020	0.044	0.087	0.136
Cosmic Rays	3.498	5.939	9.861	18.97	23.724
Total Time per Image	4.155	6.697	11.184	21.778	27.352
Total Time for entire set	84.049	66.216	56.408	59.754	58.536

Table 2.2: Average time in seconds for each step in the reduction process for 86 images provided by the PT-MoDf for different number of threads used in multi-threading. There is also available the total time required by SPADE to process the entire set of images. Calculations were performed in a virtual machine with 10GB of RAM and 8 cores.

Reduction Process	Average Time per Image (s)				
Number of Threads	1	2	4	8	10
Gain	0.005	0.008	0.012	0.019	0.041
Background	0.482	0.569	1.008	1.691	2.559
Crosstalk	0.017	0.021	0.042	0.082	0.125
Cosmic Rays	4.406	7.296	12.176	24.111	29.648
Total Time per Image	4.910	7.894	13.238	25.829	32.372
Total Time for entire set	426.702	342.273	289.770	285.913	289.001

Chapter 3

Image Analysis

In this chapter we will discuss the image analysis steps from the detection of point sources up to the identification of space debris. The algorithm is capable of performing astrometry with the 2 arcsec accuracy required by the SST in the GEO and MEO region (European Comission, 2022). SPADE makes use of the known software *Sextractor*, *Astrometry.net* and *PSFEx* as well as common packages such as *numpy* and *astropy* (Bertin & Arnouts, 1996; Bertin, 2013; Lang et al., 2010). Due to the high number of images that can be generated every night by the double telescope, SPADE was designed to use multi-threading to significantly speed up several steps of the algorithm in order to avoid clogging the pipeline during operation and to ensure real-time analysis.

3.1 Source detection - Sextractor

The first and probably the most important step is to accurately detect all sources in the image. To do this, SPADE takes advantage of the *Sextractor* software (Bertin & Arnouts, 1996). Its widespread use in optical telescope images in the last couple of decades has shown its reliability and the quality of the results obtained. The software can detect both point and extended sources. SPADE will then have the flexibility of working in both cases. This is why it was chosen over others such as DAOFIND (Stetson, 1987). Even though only point sources will be studied in our specific application, there are plans to use the telescopes for science imaging in the future which may involve extended sources such as galaxies.

The most important parameter for source detection is the detection threshold. In the astronomy community this threshold is commonly calculated based on the background signal distribution. The standard deviation of this distribution is calculated, usually denoted by the letter σ. The thresholds are then calculated in multiples of this value. The higher the value, the greater the confidence level that the detection is not due to a random effect. The usual accepted values for detection thresholds in astronomical literature are 3σ, where there is a 0.3 % chance that the observed result is due to a random effect or 5σ where there is less than a a $6{\times}10^{-5}$ % chance (Abbott et al., 2021; Schlafly et al., 2018). In SPADE we ended up choosing 3σ for the value for the threshold detection. In simpler terms, the signal must be at least 3 times the standard deviation of the background signal to be considered a detection.

Lower values of 1σ and 2σ were also considered as not all RSOs were detected with the selected threshold value due to the presence of some faint sources. By analysing the images given to us by the PT-MoD we found that with these thresholds the number of detections increased significantly when compared to 3σ and 5σ. The visual comparison between these threshold and 2σ can be seen in 3.1. This not only increases the computational cost of the pipeline but we also found that there was a great increase in false positives which propagated all the way to the end. As avoiding false positives is crucially important in this work, we decided that it was not worth to sacrifice releasing wrong information in order to detect all debris present in the image, choosing 3σ. We also note

that we did not have flat and dark frames available which did not let us correct the vignetting. This effect worsened the quality of detection in the corners for the same threshold value. Seeing that the center performed well we expect that with the full reduction process this problem will be eliminated.

In *Sextractor* this is controlled by changing DETECT_THRESH and ANALYSIS_THRESH. The first controls the threshold for a detection to actually be made and the properties calculated. The second only controls if some specific parameters are calculated such as the FWHM. Since we want to obtain information from all the sources detected, we set them equal.

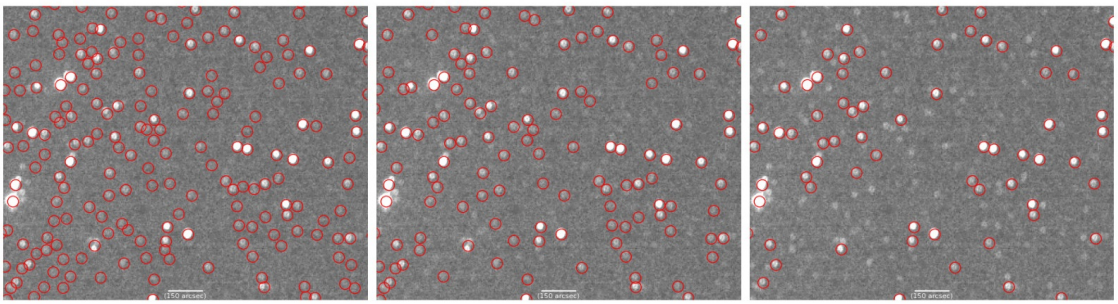

Figure 3.1: Image detail with extracted sources marked as red circles from SPADE for threshold values of 2σ, 3σ and 5σ, from left to right respectively. The image used was given by the PT-MoD at the coordinate RA=8:07:00 (h:m:s) and Dec = -5:11:42 (d:m:s), starting at 2023-02-28 20:20:18.075 UTC. We can easily notice that for smaller thresholds the number of detections increases significantly. At 5σ we observe many faint sources that are not detected. On the 2σ we observe many detections that are not present in the image. The scale is provided by the small while line which corresponds to 150 arcsec.

Another very important parameter that should not be overlooked is the DETECT_MINAREA setting. This controls the minimum number of connected pixels above the threshold to be considered a detection. This value depends on the instrument used. For this reason instead of picking a number that matched most of other cases in the literature, we tested different values to detect the maximum number of sources while avoiding false positives. We found that when this value was lower than 6, the number of detections increased greatly with the majority being false positives. For that reason we ended up choosing that value even if it meant losing some real but faint sources.

The parameters chosen for output were those necessary for analysis such as X_IMAGE, Y_IMAGE and MAG_ISOCOR with the corresponding error MAGERR_ISOCOR. These parameters of position are the baricenter of the source. This option was preferable over the brightest pixel as that allows us to have a precision superior to the pixel scale. The choice for the MAG_ISOCOR is explained in section 3.3.

Apart from that we also output the information required by *PSFEx*. These are the FLUX_RADIUS which corresponds to the radius that contains half the flux, FLUX_APER which is the flux calculated with a fixed aperture and FLUXERR_APER the corresponding error. There are also other quality parameters such as SNR_WIN which gives the SNR of the object, ELONGATION which is the elongation of the object and FLAGS which give information about certain problems that might have occurred with the object . This might be saturation or being too close to the border. The final parameter is VIGNET(15,15) which is the one we can change. This value controls the size of the sub-image, in pixels, that is saved for each detection. In SPADE we chose 15. This decision was made following *PSFEx* documentation as it is neither too small to not encompass all of the PSF but is not large enough that it generates too big of an output file and slows down significantly the processing speed or have a high risk of contamination from a near object. It serves as the default for this pipeline but it can be easily changed manually in the configuration file. Another aspect to take into account is that if a source is so close to the border that this sub-image can not be saved, SPADE will eliminate it. This is another incentive to decrease the value as much as possible to avoid eliminating debris that appear very close to the border. This

discussion is looked further into in subsection 3.6.3. All these parameters can be easily seen in table 3.1.

Table 3.1: Sextractor configuration file settings changed from the default file (left) and output parameters (right).

Setting	Value
CATALOG_TYPE	FITS_1.0/ FITS_LDAC
DETECT_TYPE	CCD
DETECT_MINAREA	6
DETECT_THRESH	3
ANALYSIS_THRESH	3

Output parameters	
NUMBER	FLUX_ISOCOR
MAG_ISOCOR	MAGERR_ISOCOR
FLUX_APER	FLUXERR_APER
X_IMAGE	Y_IMAGE
FLAGS	FWHM_IMAGE
ELONGATION	FLUX_RADIUS
SNR_WIN	VIGNET(15,15)

3.2 Plate solving - Astrometry.net

The most important information for SST purposes is astrometic measurements of sources. Precision in this parameter is not only vital to make sure the correct object is detected but also for validation of collision avoidance algorithms between space debris and active satellites. It also enables the use of different techniques such as image stacking or differencing which can lead to improvements in various parameters such as the SNR and magnitude or even the detection of transient objects (Patterson, 2018).

To perform this vital step in SPADE, the widely known *Astrometry.net* was used (Lang et al., 2010). The widespread use of this software in the astronomical area is proof of the consistency and reliability of its results. This software makes use of index files built from catalogues such as the 2MASS and the Tycho2 to discover the area of the sky that better matches with our images. This software uses pattern recognition. It compares the shape of sets of 4 stars (quads) with the ones saved in the indexes to find the best match in the sky. It then corrects for image distortion by using a 3^{rd} order polynomial correction, vital for big FoV like ours where linear approximations do not work as well. This process can be assisted by supplying the software with information about the telescope and the images such as FoV, center coordinates and image scale. This can greatly decrease the processing time for this step. All these parameters can be easily controlled in the configuration file to fit different telescopes.

Depending on the area of the sky observed and the threshold value used the number of detected sources in each image can, as previously seen, increase significantly. This will naturally lead to an increase in the time needed for plate solving, possibly clogging the pipeline or reaching the point where no solution is found in the allocated time. This would mean that a given set of images would not be analysed leading to the loss of information and useful night time. To avoid this, SPADE limits the number of sources fed to *Astrometry.net* to 500. We decided to select the sources with the highest SNR in the image. This was the parameter chosen because we expect these objects to have a better defined PSF which will lead to a better precision of the source position. Of course, SPADE also eliminates all saturated sources. This selection potentially allows for lower threshold levels to be used and analyse denser star fields without the need to sacrifice having long computational times. We have decided not to do so to avoid false positives in other steps. This decision is further discussed in subsection 3.6.2.

To analyse the quality of this step in our pipeline, we compared our coordinates with their match in the UCAC5 catalogue. We calculated both the angular difference between them given by equation 1.3 as well as the difference in the RA and Dec values. This was done both for all images given by the PT-MoD (figures 3.2 and 3.3) as well as for each individual set of 4 images (figures 3.4 and 3.5). We decided to use the FWHM as the precision parameter of our detections. Since this value is much larger than the catalogue objects precision, this was the maximum distance to consider a match.

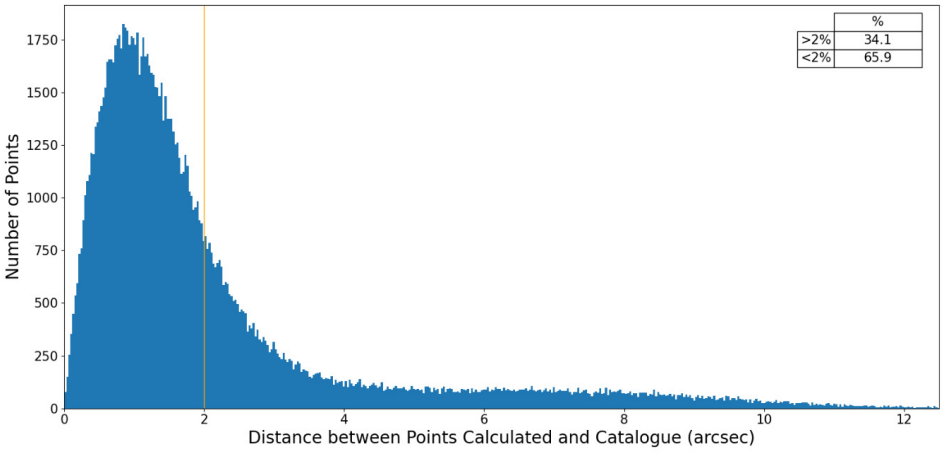

Figure 3.2: Angular distance between calculated coordinates and their match in the UCAC5 catalogue for all 86 images given by the PT-MoD, in arcseconds. Images were analysed with a 3σ threshold value.

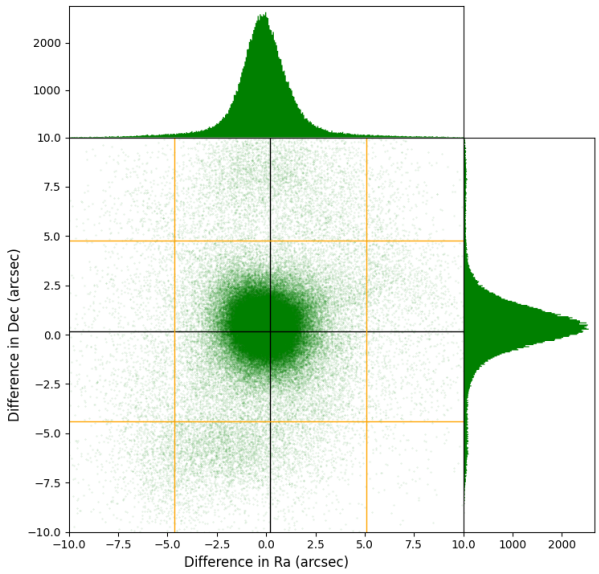

Figure 3.3: Difference between Calculated coordinates and their match in the UCAC5 catalogue for all images given by the PT-MoD, given in arcseconds with Declination on the Y axis and Right Ascension on the X axis. The mean values and standard deviation of both axis are marked with black and orange lines respectively. Images were analysed with a 3σ threshold value.

Analysing figure 3.2, we can see that angular distances are mostly (85.2%) below the pixel size ($\approx$ 4.6 arcsec). The required precision in astrometry for SST usage in the GEO and MEO region is 2 arcsec (European Comission, 2022). A majority of detections (65.9%) follow this requirement with the median value situated at 1.450 arcsec. This is a good indicator of the results obtained. To make sure, SPADE will be tested with calibration objects when the double telescope setup becomes fully operational.

When looking at the RA and Dec values separately in figure 3.3 we can observe that the distribution is similar in both axis. When analysing these distributions in detail we obtain mean values of (0.2258 ± 0.0006) and (0.1932 ± 0.0005) arcsec, and standard deviations of 4.3701 and 4.6694 arsec for Dec and RA respectively.

We expected the mean values to be 0. The difference can either be due to a bias, or simply the instrument limit. The standard deviations were expected to be nearly equal. There is a slight increase in the RA direction which can be due to an image factor or simply limited by the instrument. A possible explanation for the difference in standard deviations could be due to the fact that the length of RA circles decreases as we increase the value of Dec. This means that each pixel will represent a bigger angular portion of the sky. This effect varies with the cos(Dec), which at the declination that is being observed in this data-set (GEO belt) can be disregarded. Another aspect that is visible in figure 3.3 is the appearance of two disperse groups of detections with an offset in declination both positive and negative. To be able to correctly understand what originates these problems we analysed every set of 4 images individually which can be seen in figures 3.4 and 3.5. From both figures we can immediately understand that there are some sets with very different behaviours.

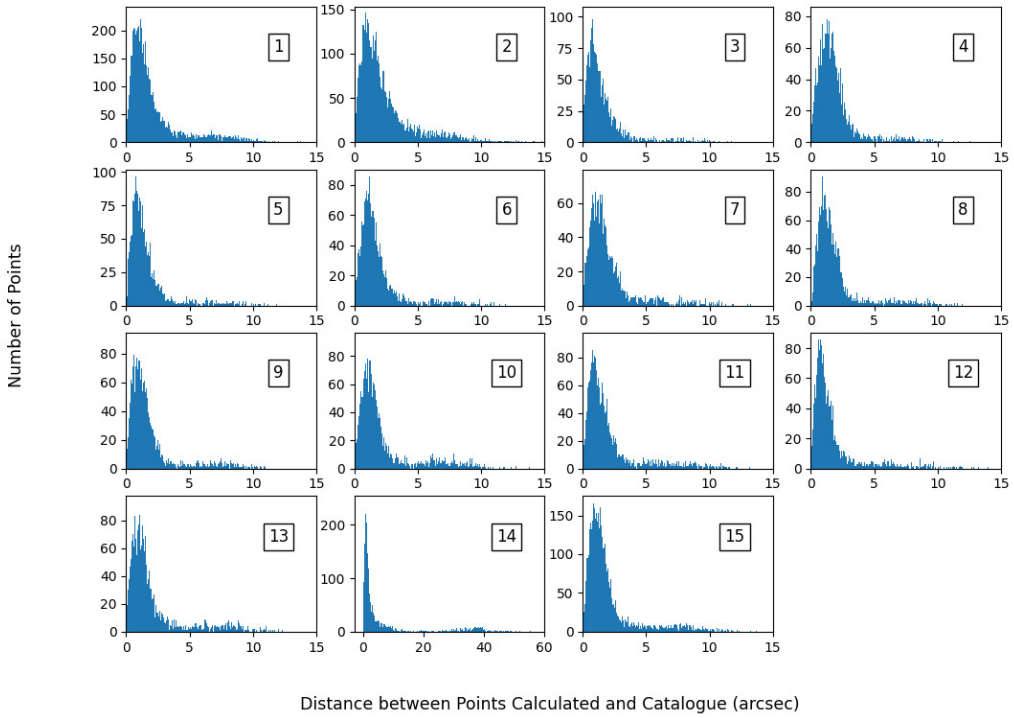

Figure 3.4: Angular distance between calculated coordinates and their match in the UCAC5 catalogue for all 15 images sets given by the PT-MoD, in arcseconds. Image sets are organized from left to right and from top to bottom.

The set that stands out the most is set 14. In figures 3.4 and 3.5 we can observe a second distribution appearing nearly at a 40 arcsec difference from the center. This is due to the effect visible in figure 1.7 (left) (in page 9) where every source appears duplicated. This effect was probably caused by the sensor shaking due to the wind. This means that we will have a group centered near (0,0) and another group centered at the difference due to the shaking. Even though it affects both coordinates, this difference happens to be bigger in the RA direction. This explains why the standard deviation is bigger and why the mean value is not as closer to 0. This only

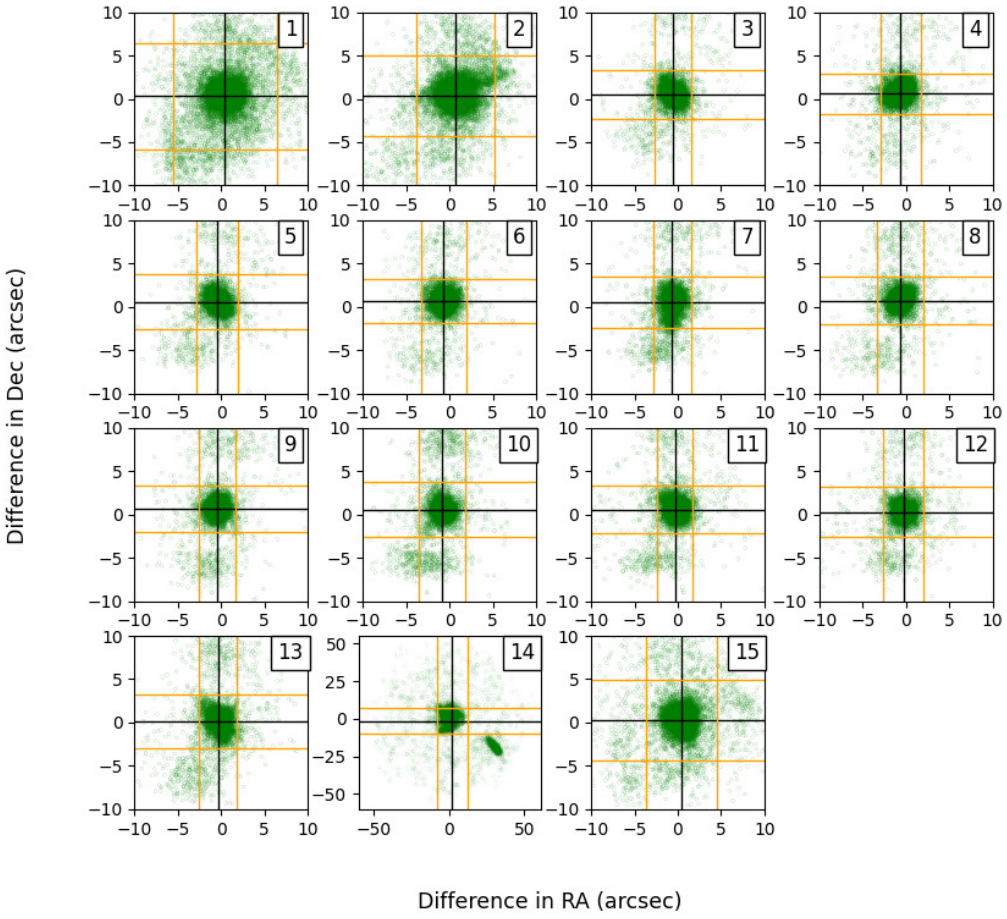

Figure 3.5: Difference between Calculated coordinates and their match in the UCAC5 catalogue for all images sets given by the PT-MoD, given in arcseconds with Declination on the Y axis and Right Ascension on the X axis. The mean values and standard deviation of both axis are marked with black and orange lines respectively. Image sets are organized from left to right and from top to bottom. Set 14 has a zoomed out view so that the second group created by the sensor shaking is visible.

---

occurred for 1 image out of the entire data-set so it isn't a recurring problem but still needs to be thought of. The PT-MoD telescope is made to be mobile and is built in a container where the foundation of the sensor is the same as the dome. This does not protect it from winds effects. In our double telescope setup, the foundation of the sensor is separated from the foundation of the dome to reduce these exact situations. Removing this image from consideration, the standard deviation of the rest of the data-set drops to 3.721 and 3.351 arcsec, and the mean values change to (0.396 $\pm$ 0.001) and (-0.0738 $\pm$ 0.0002) arcsec for Dec and RA respectively.

Even though the values improve significantly for RA, the mean value of Dec increases and now the Dec standard deviation is the one visibly bigger. From figure 3.3 we can notice that the formation of two groups with an offset in declination happens for all sets. This effect may result from the appearance of "donut" and 'bean" shaped sources in the images visible in figure 1.5 (in page 8). These are caused by the optical system not being correctly focused and collimated respectively. These effects worsen in the top right corner of every image as can be seen in figure 3.6. The first effect should be the least problematic as it is expected to be symmetric in all

directions which should keep the photo-center close to the same. This will only slightly increase the distribution's standard deviation in both directions as the PSF will be deteriorated. The second effect is more problematic as the effect is larger on the vertical axis, which is aligned with the declination, and is not symmetrical. This will originate an offset both downwards and upwards, with a prevalence of the second as can be seen in figure 3.6. The effect on the PSF of the image will be seen in figure 3.8 in page 28. With that view, it is clearer how this offset originates.

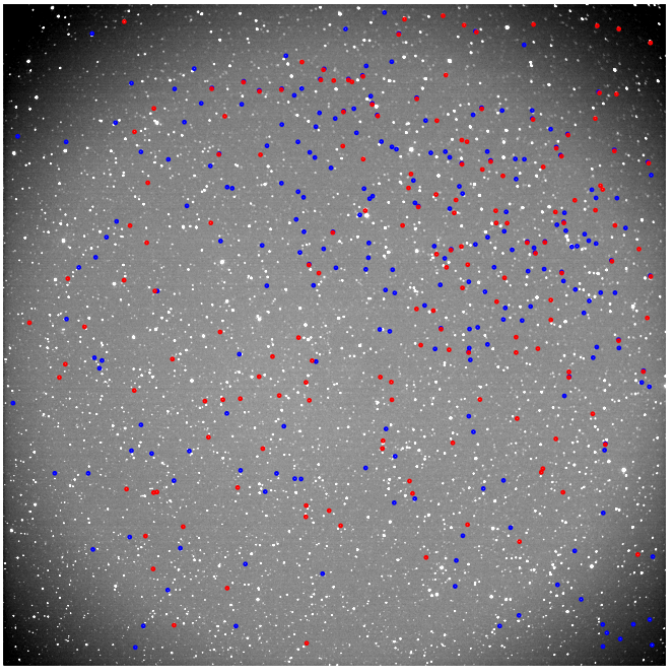

Figure 3.6: Detections with a difference in Dec bigger than 3 arsec are marked as blue and detections with a difference smaller than -3 arcsec are marked as red. We can also notice that the effect happens throughout the image as expected from a distribution but it is clear that the declination bias is predominant in the top right corner where the collimating effect is stronger, with a prevalence for positive bias over negative bias cases.

There is one last effect which is harder to see but happens in a majority of the sets, appearing in sets 3, 4, 7, 9, 11, 12, 13 and 15. In figure 3.5 we can notice that there is a visible elongation in the declination axis in these sets, especially in sets 7 and 13. This is caused by the sources stretching during the exposure in some images, like a RSO in movement. This effect can be seen in figure 1.6 in page 9. Since this only happens for the first image of each set, we can not conclude that it is due to wind like the first effect as that would happen randomly. The hypothesis is that this effect is originated by the sensor beginning its exposure before the telescope completely stops on the target. This leads to the source stretching during the small time in which the telescope is still in motion. The first thought might be that the telescope has a fixed time between fields and it is not able to move to the next field in time. This is not true as the time difference between different sets varies from set to set. The next reason might be that the telescope needs to move in both axis (RA and Dec) and slows down more than expected. This is not true as it happens for both cases where only Dec movement is performed (ex: set 4) and where both movements are perfomed (ex: set 3). Another reason might be that this can happen if the distance travelled by the telescope between fields is too big. This is not true as it does not happen for set 14 which changes to a completely different area, but happens for set 3 that has less than a 5° change in Dec. We can not find a pattern to explain this appearance so our hypothesis is that the time control is too tight not taking into account the variance in the time needed for the movement. This will lead to this effect happening in half the sets. This effect only happens in the vertical

axis. As we do not operate the telescope, we can not know for certain but we hypothesise that the setup firstly moves in the RA axis and then in the Dec axis. By starting the acquisition early, the telescope will still be moving only in this axis which will result in no effect in the RA direction.

Even though good information can still be taken from these sets, it can be looked into to make sure these effects are completely removed so we can obtain the best possible results in the future operation of the double telescope. Even though these effects are negative to the images, they have a positive influence as they served as a good test for SPADE as even in these conditions, some sets have standard deviations smaller than 2 in both axis, as needed for SST.

There is one last piece of information that we can take from analysing these figures. If we look at set 14 in figure 3.5, which has a zoomed out view, we can see that there is a formation of a perfect circle of green dots which marks the threshold (FWHM) used for the accepted distance in the catalogue comparison step explained in section 1.6. It is immediately visible that this value is much larger than the standard deviation observed discussed previously. This leads us to conclude that this value may be lowered.

There are two options to decide this value: a fixed value based on a parameter such as the maximum error allowed by the SST for GEO positions (2 arcsec) or a variable scale such as a selection of a percentile of the distance distribution. The first option would seem as a very good option as the distribution seen in our images is situated almost perfectly in that range and it would also seem to eliminate the problems previously discussed. But choosing a fixed value would not guarantee that we would end up with a good distribution. This means that we could be lead to wrong conclusions based on a flawed distribution. A percentile approach would have the major advantage of adjusting to every image, protecting SPADE from bad images advancing further. The difficulty comes with the definition of what percentile to keep. We calculated the percentage of detections inside a 3 arcsec distance radius for each set of images. We found that to be the average radius observed in figure 3.5 that preserved the majority of detections while removing the effects that were discussed. From those values we calculated the median in order to lessen the effect from the worst cases and obtained a value of 85%, which is the percentage used in SPADE.

With this correction and without the first image from set 14, the standard deviation of the data-set drops to 1.178 and 1.174 arcsec for Dec and RA respectively. The mean values do not change significantly with (0.382 ± 0.001) and (0.0815 ± 0.0002) for Dec and RA respectively. These values show that while the effect is worsened for the corners it also applies to the center sources. This leads to the standard deviation decreasing while keeping the bias in the Dec value. A visual representation of this can be seen in the asymmetry of the average PSF in figure 3.8, page 28. The two peaks in the PSF, formed due to the focus and collimation effects, are aligned with the y axis, or the Dec. This effect is not symmetrical, the peak which is largest in declination is higher in value. This will move the source barycenter to bigger Dec values and thus creating the bias.

This process can now be used as quality control for the individual sets by analysing the distance that corresponds to that percentile. From the sets available from PT-MoD, two jump out immediately with values much larger than the rest: set 2 with 4.648 and set 14 with 7.993 pixels in comparison with the median value of 2.673 pixels. In figure 3.7 we can see the new distributions, with set 2 and 14 in comparison with set 3, a typical set. We can immediately see that they are completely different and that the distributions are more problematic.

3.3 Photometry - PSFEx

Photometry is the measurement of an object's brightness. Astronomers have long used this property to make determinations such as distance or temperature of celestial objects like stars, asteroids or galaxies. This property was quickly thought to be used for satellite observations to test in order to obtain important parameters such as their rotational speed from the variation in brightness with time or the determination of the object composition with the observation with different color filters (Gasdia et al., 2017; Zhao et al., 2021). This is more easily said than done but there is an intensive study within the space debris community to quickly develop different

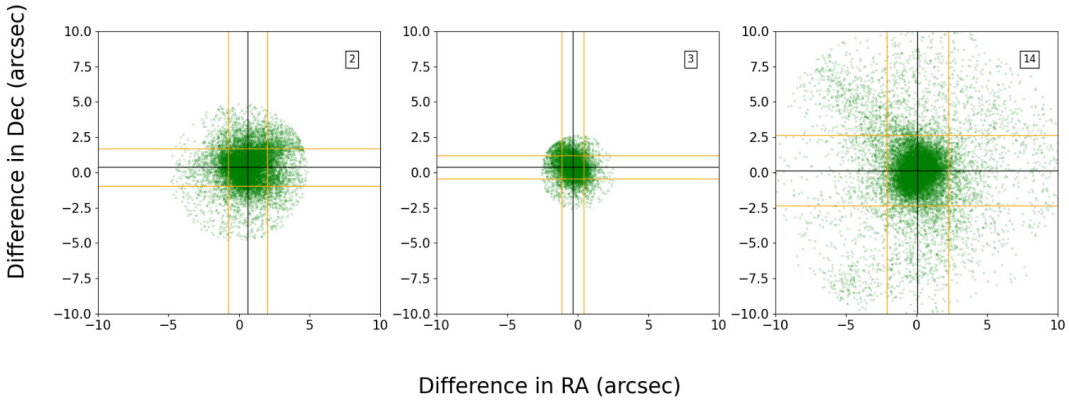

Figure 3.7: Difference between calculated coordinates and their match in the UCAC5 catalogue for image sets 2, 3 and 14 given by the PT-MoD. Dec on the Y axis and RA on the X axis are in arcsec. The mean values and standard deviation of both axis are marked with black and orange lines, respectively. Only the 85% sources with the smallest distance are marked in this graph.

---

tools such as light curve time analysis in Piergentili et al. (2021) and different filter and phase angle analysis in Zigo et al. (2019). Even though photometry is not requested by the EU-SST, an implementation in SPADE could help future applications.

In order to correctly perform photometry on our sources, we need to calibrate our instrumental magnitudes. There are a number of possible solutions for this calibration process. One could be observing standard calibration stars such as Vega and study the relationships between image counts, exposure time, air-mass and star magnitude. In this way, we could completely characterize the instrument and enable a faster processing speed for our pipeline. The disadvantage of this method is that it requires a long time to observe a number of calibration stars that would cover the magnitude range observed within the telescope lifetime. Another problem is that this method would be extremely vulnerable to atmospheric changes. This could be avoided for science images as they would only be taken in good conditions. Seeing that the telescope can be used in relatively harsh conditions (for SST operation) this possibility can not be used. For the double telescope we decided that the calibration would be made for every single image by comparing the instrumental magnitudes of our image to the magnitude of the matched stars from a catalogue. This creates a solution that can be used immediately at the start of the operation of the double telescope.

Since the scale of magnitudes is a relative system we expect that the variation in the instrumental magnitudes will be the same as the real magnitudes. This means that the difference between these two values will be constant in the image, usually known as the zero-point. An important note is that we need a catalogue with magnitudes of the same filter as the one used in our images as not all stars will have the same spectral energy distribution. In our case, we have the common Johnson-Cousins filters. For white light (no filter), we use the Gaia magnitude (G) available in the UCAC5 catalogue, as the filter used in this mission is similar to the light curve of our sensor, figure 1.4 in page 8.

Sextractor has the ability to perform photometry with various options. The main ones are isophotal and aperture photometry. The isophotal method calculates the flux by summing all pixels which are above the threshold, changing the number of pixels for different detections. Aperture instead uses a fixed circular aperture and adds all pixels within that zone, being fixed independent of the source being strong or weak. We decided on using the isophotal method as that would better adapt to the different zones in our large FoV. This method is also more resilient to possible effects that may affect our images like the ones seen in our data-set. The isophotal method disadvantage

is that it loses a fraction of the flux on the tail of the distribution. *Sextractor* corrects this effect by assuming that the distribution are Gaussian, working best for point-sources Holwerda, 2005. This new magnitude is called MAG_ISOCOR which is the one chosen in SPADE.

These methods were created to optimize photometry for extended sources which was the main purpose for the creation of *Sextractor* (Holwerda, 2005). According to Annunziatella et al. (2013) these methods lack precision when applied to point sources such as stars or RSOs which are the focus of this work. To solve this issue, a new tool was developed to assist *Sextractor*, called *PSFEx* (Bertin, 2013). This software calculates the average PSF in the image, which can be fed back to *Sextractor* to perform PSF-fitting photometry, decreasing the error for point sources. We plan to develop a new tool in the near future to characterize space debris based on the analysis of their light curve. For this to be possible we want to be able to be able to observe the minimum possible variation in an object magnitude over time. If we increase the precision of our photometry, we will be able to study a larger number of debris. An example of an image PSF obtained from SPADE can be seen in figure 3.8. As we can see, the PSF is significantly deformed, even forming two peaks. This is due to the effects previously discussed about the focus and collimation of the optical system. We can also note that the two peaks are not balanced, as one if higher than the other and alligned with the vertical axis. This explains the bias we observed in the Dec direction in the section 3.2. For this reason, the PSF-fitting photometry does not provide the best results in our images. This result does not let us truly test this method with SPADE, leaving it to future work. The rest of the analysis will be done with MAG_ISOCOR magnitudes.

In figure 3.9 we can see two examples of the catalogue magnitudes as function of the instrumental magnitudes for the image with the highest number of sources and the image with the lowest number.

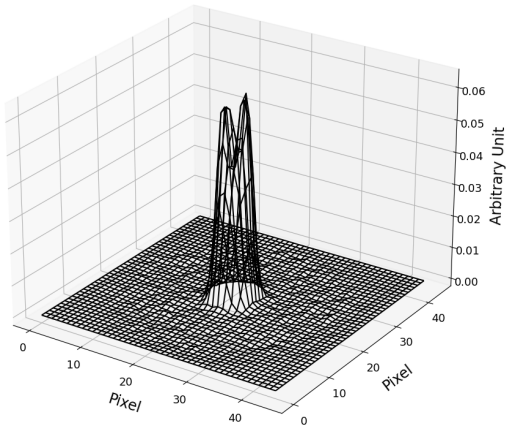

Figure 3.8: Average Point Spread Function (PSF) of the first image from set 1 given by the PT-MoD, with a (45×45) vignet. Sources with unusual FWHM values, low SNR, and saturated sources are excluded from this calculation.

As the CMOS sensor used in the telescope is linear we expect the instrumental magnitude and the true magnitude to be perfectly correlated. In fact, the CMOS sensor becomes non-linear before saturation, which will slowly increase the slope for lower magnitudes (stronger sources), as can be seen in figure 3.9. For this reason, we will not use this zone for the fit. On the other hand, we can observe that for higher magnitudes (fainter sources) there is an increase in the spread of the function, decreasing the quality of the fit. On the left of figure 3.9 we can observe that the sources with smaller distances have smaller dispersion. This immediately jumps out as a possible parameter to select the sources in order to improve the calibration process. For this reason SPADE maintains only the 85% percentile selected in section 3.2. The new distributions

can be seen on the right of figure 3.9. It is visible that while some dispersion remains it is much smaller. The zeropoint for both distributions are (22.53 ± 0.09) and (22.8 ± 0.1) respectively. We expect to improve these results with *PSFEx* but are a good sign for future applications. With these calibration values the maximum magnitude observed was 15.12 mag from image 1 of set 1.

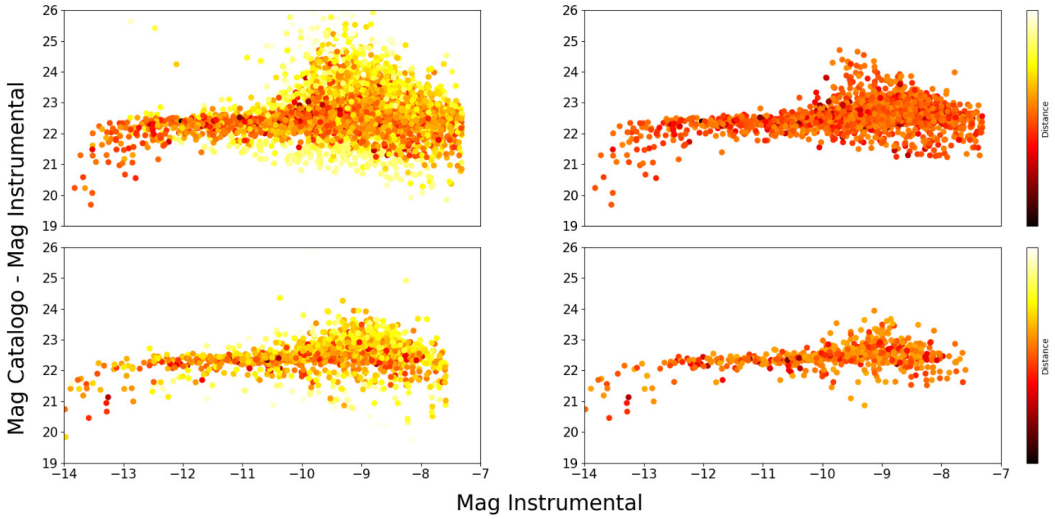

Figure 3.9: Catalogued Magnitude and Instrumental Magnituded difference (Y axis) vs Instrumental Magnitude (X axis) for two different images from the PT-MoD. The top figures are from image 1 from set 1 and the bottom figures are from image 2 from set 13. These were chosen because they are the images with the highest (4713) and the lowest (1443) number of sources respectively. The left figures are the total detections and the right figures only the sources selected with the 85% percentile of distance to the catalogue match. These figures have a colormap to show the distance between the detected source and the catalogue match, going from dark (small distances) to bright (bigger distances). The colormaps are shared for both figures of the same image.

3.4 Debris Classification

There are a multitude of studies investigating different ways on how to identify RSO in optical images. Most methods attempt to take advantage of the ever-present technology of machine-learning such as Jordan et al. (2022, 2023) while others try to find innovative and clever ways to tackle the problem such as Zuehlke et al. (2021) with the use of optical flow. We wanted to create a solution that could be used immediately in PASO as well as in other future sites. This led us away from machine-learning methods which require a large amount of data at the beginning to train our models which would delay even further our acquisition process, and led us onto computer vision methods which are also common in examples such as Cegarra Polo et al. (2022).

The telescope will compensate for Earth's rotation keeping stars as point sources. Satellites however, move differently than stars. The result will be that RSO will move from image to image and the PSF will elongate during the exposure. For that reason, one possible method to separate stars from artificial satellites in our images is to check if there is movement in a set of images taken in sequence with a small interval. The expected movement will depend on the type of orbit we are observing, mainly LEO, MEO, and GEO, as they will differ in angular speeds and direction.

In GEO orbits we expect a 24h period which will translate into 15 arcsec/second movement in our images, or 3.26 pixels/second with a 4.6 arcsec/pixel scale. We also expect them to have a constant value of declination for active satellites over time. The MEO and LEO orbits have a larger altitude interval which implies a difference in the angular velocities between different objects in the same type of orbit. These orbits can also move in every direction. On average, LEO have an angular velocity of around 1000 arcsec/second or 217 pixels/second. In MEO orbits the large

altitude interval, 2000 km to 35786 km, leads to a wide range of angular velocities. If we look at specific cases like the GPS system, they have an angular velocity of around 30 arcsec/second or 6.5 pixels/second (Silha et al., 2014). With short exposure times, GEO and MEO detections can be approximately considered as point sources, as the values are comparable to the FWHM produced by the optical system. On the other hand, faster angular velocities in LEO will make RSOs appear as lines in our images instead of point sources. This makes it easier to identify visually in our images but it will also add a level of complexity to the debris detection. To avoid false positives and to be able to properly create an orbit prediction, we require a minimum of 3 consecutive detections according to the expected movement. Due to how fast a LEO passes our FoV it may become hard to obtain three consecutive detections on the same field. Not only that, it also forces the implementation of line detection tools in SPADE.

At the present SPADE is focused on analysing the GEO and MEO where we can assume point sources in our images. The main method used in SPADE relies on image cross-referencing where we compare different images taken from the same field with a small time gap in between. There is an additional method also implemented which is catalogue comparison. In this second method we compare our detections with a star catalogue and assume that the additional detections are RSO. This method is much worse and will only be used as a possibly safety tool in the case that only one or two images are available for some special reason. These methods will be explained in the following subsections.

3.4.1 Image Cross-referencing

In SPADE the main debris detection method is based on detection cross-referencing between consecutive images to separate objects that remain in the same place (stars) from objects that move from image to image (RSOs). The usual operation will involve taking sets of 4 or 6 images for each field.

In theory by cross-referencing detections from all images of the same set we will be left with "unique" detections which should be RSOs. In practice not all objects that "move" from consecutive images are RSOs as false positives may occur in cases such as cosmic rays that were not properly removed in the reduction process, faint sources that only appear in one image due to atmospherical effects or simply false detections from the pipeline that may occur. For this reason we advise higher thresholds for the source detection step of SPADE to lower the chance of false positives in the end of this step. Seeing that we are comparing objects detected in our images, we used half the highest median FWHM of the 2 images as the maximum distance. We find that this is the minimum distance to differentiate between two distributions. The decision made in sections 3.2 and 3.3 to lower the threshold in the comparison method was not made again as that could easily cause the appearance of false positives.

For SPADE to identify an RSO a 3 tests setup was implemented. The first test requires a minimum of 3 detections in different images which can be consecutive (ex: 1, 2, 3) or missing an intermediate value (ex: 1, 2, 4). Seeing that our data-set involves sets of 4, there can only be one error before the RSO is discarded.

SPADE then checks for the angular distance travelled between images in celestial coordinates (RA and Dec). This was not done in image coordinates (X and Y) to protect SPADE from misalignments that may occur with the telescope during operation. We expect an RSO to have constant speed in the time-frame of our images so we expect a similar change in position in each frame. Seeing that there is always some error in our position value, there will always be some slight variation between images. From analysing images given to us by the PT-MoD, we noticed that RSOs would always have less than a 5% difference between the highest and lowest distance between consecutive images so we chose that as our threshold parameter. With more and more images, this parameter can be fine tuned if it is shown that it is too strict and we can loosen it to capture more debris or it is causing too much false positives and we need to tighten it up even if it means to lose some detections. We also need to take into account the effects present in the images that were offered to us by the PT-MoD which could allow us to reduce this value with our own future images.

The third and final test analyses direction and order of "unique" detections. A normal RSO will cross our FoV approximately in a straight line. SPADE calculates the angle corresponding to the change of direction between consecutive images. This parameter is quite sensitive to small changes so it needs to be looser. To decide the value to define as default we followed the thought process for the distance parameter and chose a value of 8° as we found that value was the limit until we started to observe false positives in the available images. Like the previous one, this parameter will evolve as the pipeline is used to perfect the system. The points also need to be in order for SPADE to accept them.

Every test and parameter in this verification step can be enabled or disabled and controlled easily in our configuration file to better suit the operator needs. These conditions can be visually seen in figure 3.10.

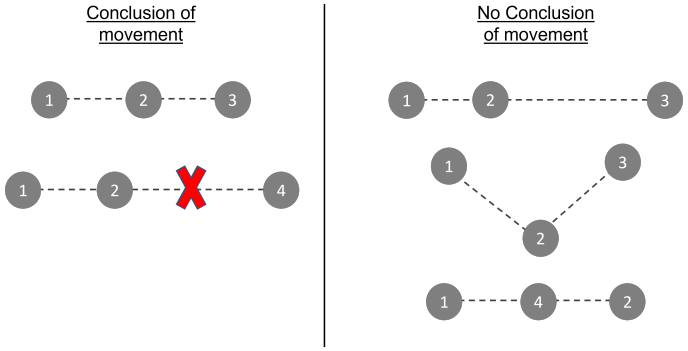

Figure 3.10: Conditions for RSO detection. There must be a minimum of 3 Detections that follow a straight path, in the direction expected from each orbit in the correct order. We allow an intermediate detection to be lost which can happen due in specials cases such as due to atmospheric effects or mixing with a star in its path, if the sources are in the correct position.

3.4.2 Catalog Comparison

The second method studied was the comparison of our detections with a star catalogue to check which unexpected objects are appearing in our images. To have good results we need to have a complete catalogue up to the magnitude that our telescope can observe to avoid false negatives in fainter sources and good astrometric precision for each source so that it does not limit SPADE's precision. As seen in section 1.6, SPADE uses the UCAC5 catalogue for this match which fits both requirements. This solution is going to be used when we only have a single image of a given field. The PT-MoD available images originated too many false detections to make this method viable so it could not be tested thoroughly. When the double telescope starts operating this option will be looked into again with the possibility of using multivariate statistics.

3.5 Sattelite Identification

After detecting a RSO in our images, the next step is to try and match it with a known object. This is done by propagating TLEs from a catalogue of objects to see which should be visible in our image and if they are close to our detection. We update our TLEs everyday from the Celestrak website, a standard for the SST community. In figure 3.11 we can see the predicted position for every object in the GEO Protected Zone Plus (GPZ+) from the beginning of the first image to the end of the last. The GEO active line is clearly visible near Dec = -5° as well as the ring of inactive satellites. We can also see that the survey could have been optimized to detect more debris, as some fields do not have any in the region while there are some regions with a larger amount. This image could be a tool to assist the telescope's operation in the future.

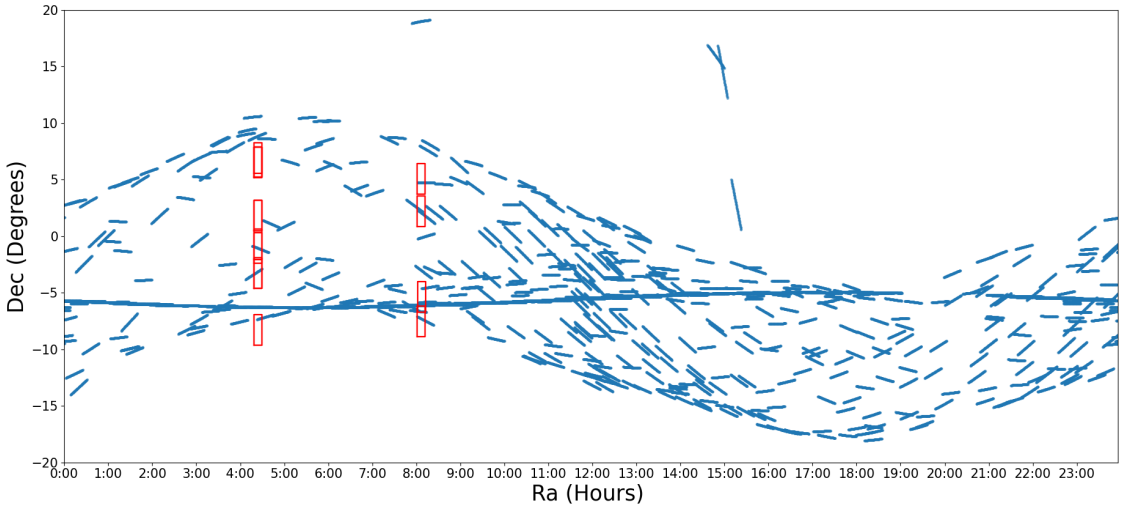

Figure 3.11: Satellite predicted position with the TLEs from the GPZ+ made available by Celestrak for day 2023-02-28 between the beginning of the first exposure and end of the last are marked as blue dots. The fields observed in the images given by the PT-MoD are marked as red.

This step is very important to help us to refine our pipeline during this initial stage as there may be objects that although present in the image are not detected as well as enable us to possibly give more information to the client. In figure 3.12 we can see an example of this where only 2 out of the 5 expected objects were detected. We noticed that from the three missing satellite only the bottom one was visible at a very faint level whereas the other two were not present in the images. This result shows a pipeline limit by not detecting very faint sources in order to increase trust in our results. We also searched an explanation about these two missing objects. Our first thought was that the TLEs for these GEOs were old, originating a large error when propagated. The oldest of the two was just 4 days old, which is not very significant for a GEO orbit and for the FoV that we are observing. The second hypothesis was that there was some problem in the propagation software implemented in SPADE. But after comparing with other softwares such as Stellarium and GPredict they matched our results. We concluded that they are just too faint, not showing in the short exposure used in these images.

When analysing the entire data-set we obtained the results presented in table 3.2. We observe that SPADE performs poorly detecting only 7/21 of the expected debris, a 33% efficiency. When observed individually we can find an explanation for this low value. In 7 cases the debris is so dim that it is not observed in the image with the exposure time used, which means that SPADE will never be able to detect them. We also noticed that there is one case where the debris is just at the border of the image which was eliminated to increase precision. The last reason is due to the debris passing by a star in its trajectory which happened in 2 cases. SPADE does not detect the debris as it mixes with the star. As we have discussed, the minimum number of detections is 3. If this effect happens twice in our 4-images sets or simultaneously with another problem such as sensor trembling, the debris becomes unidentified. For this reason, we propose to increase the number of images taken for each field from 4 to 6, to possibly eliminate this problem. If we eliminate these cases, SPADE identifies 7/11 times, or 63.6 %. These results prove that SPADE is capable of retrieving a majority of the debris even in cases where the images have a number of negative effects. When these issues are corrected we expect SPADE to obtain even better results. The 4 undetected RSOs are all due to being faint sources which are below the threshold value, showing the limits of SPADE. We are satisfied with the results as that was the compromised made to avoid false positives.

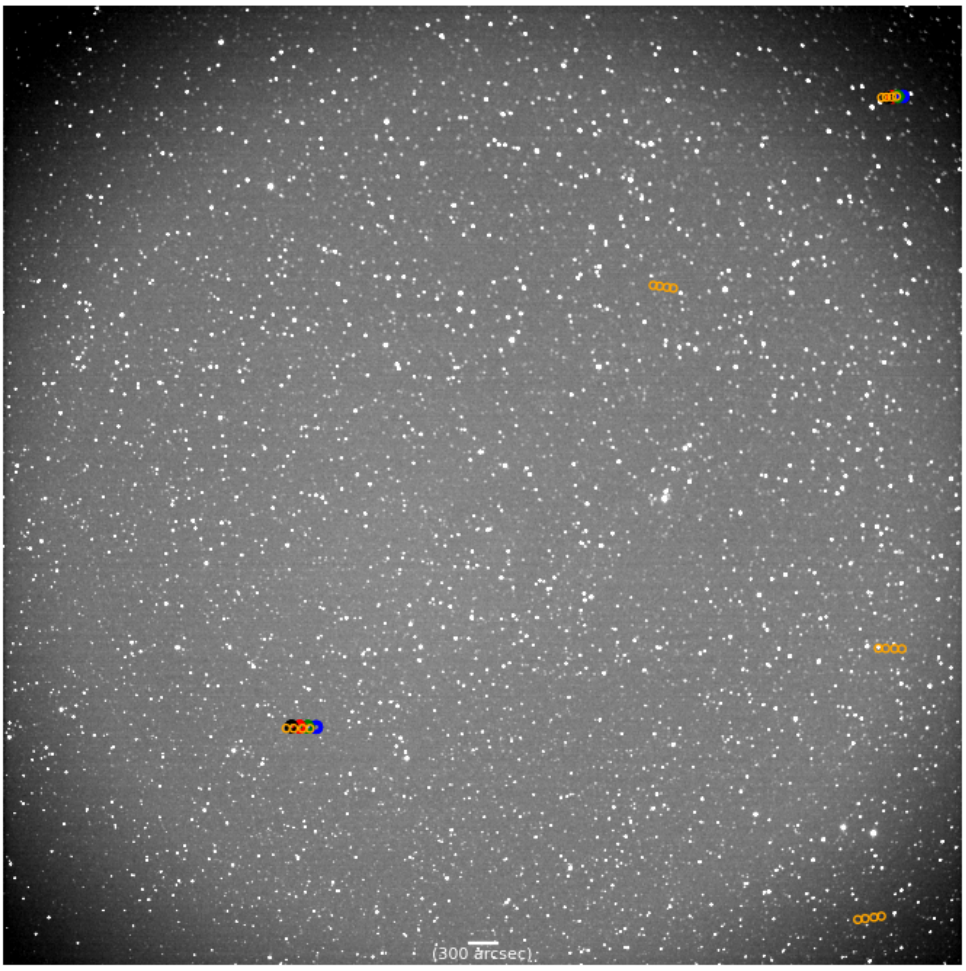

Figure 3.12: Graphical representation of output example of SPADE for set 1 of the data-set given to us by the PT-MoD, at coordinates RA = 8:07:00 and Dec = -5°11'42" starting at 2023-02-28 20:20:12.439 UTC. The detections are marked with a line of coloured circles with blue, green, red and black in order and the expected position of satellites from TLE propagation marked with orange circles. In this image we can see that SPADE detected 2 out of 5 expected debris. The scale is provided by the small while line which corresponds to 300 arcsec.

Table 3.2: Expected number of expected and detected of satellites in each set of images given by the PT-MoD, according to the TLEs taken from Celestrak for the corresponding day. No false positives were found in any set. (E - Expected, D - Detected)

Satellites		Set															
		1	2	3	4	5	6	7	8	9	10	11	12	13	14	15	Total
Total	D	2	1	2	1	0	0	0	0	1	0	0	0	0	0	0	7
	E	5	1	4	4	1	1	0	0	1	0	1	0	1	0	2	21
Active	D	0	0	0	0	0	0	0	0	0	0	0	0	0	0	0	0
	E	1	0	0	1	0	1	0	0	0	0	0	0	0	0	0	3
Inactive	D	2	1	2	1	0	0	0	0	1	0	0	0	0	0	0	7
	E	4	1	4	3	1	0	0	0	1	0	1	0	1	0	2	18

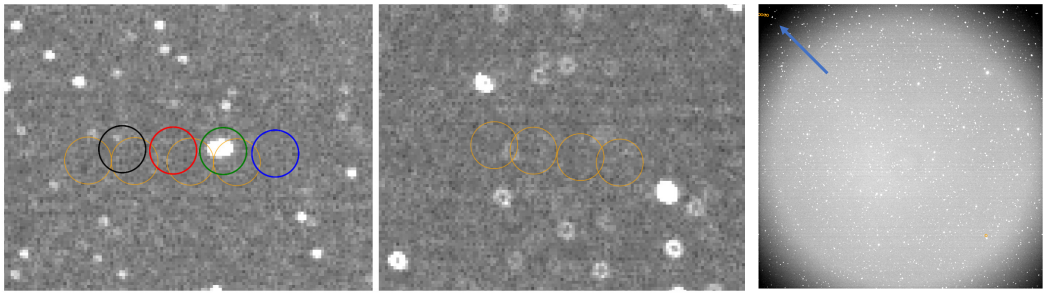

Figure 3.13: Examples of the problems that decrease the number of detections of SPADE. On the two left images we can observe the difference between a visible RSO and one not present with the expected positions marked as orange dots and the detected positions marked as blue, orange, red and black. On the right-most image we can see the problem where the source is too close to the border on the top-left corner.

3.6 Time Analysis

In this section we evaluate the time spent in each step of the image analysis process and the effect of incorporating multi-threading. These values will help us decide which steps should be upgraded first if SPADE needs to operate faster and what hardware components should be prioritized (number of cores vs RAM). For this analysis we only used the images given to us by the PT-MoD as they are better aliases of the images we expect to obtain in the future by the double telescope. This is because they have very similar FoV and a similar equipment magnitude limit. Calculations were performed in a virtual machine created on my personal computer with 10GB of RAM and 8 cores with a AMD Ryzen 5 4600H with Radeon Graphics 3.00 GHz processor.

3.6.1 Source Detection

The first step is source detection with *Sextractor*. In this step we needed to create two different output files: FITS, FITS_LDAC required for the various steps in the pipeline, previously discussed in 3.1. The first option would be to run *Sextractor* once for each output, which we will call the old version. In reality the second file contains all the information that is given by the first. For this reason we may avoid using *Sextractor* an additional time and save some precious seconds. We will call this option the upgraded version. We calculated the time taken for this step for the two different approaches. These values can be seen in table 3.3.

Firstly, when comparing the different versions, we can clearly see the improvement on all levels of multi-threading from the old to the upgraded version. On the 8 threads case this originated a decrease of more than 2 times in the time needed for the entire data-set.

The second aspect to note is that the time taken for a single image increases as we increase the number of threads analogous to what was observed previously in tables 2.1 and 2.2. This is expected as the computer will have to divide its resources through the threads, slowing down the individual process. This effect is smaller than the increase due to having multiple images being analysed in parallel. This can be seen when looking at the time taken for all 86 images. In both cases this time decreases as we increase the number of threads, to the best case of 8 threads. In the this case the time is smaller by a factor bigger than 4 compared with the no multi-threading case. In the 10 threads case the time needed for the entire data-set goes up again, due to surpassing the number of cores available to the machine. These results support the idea from section 2.3, in agreement with Subramaniam (2011) that the optimal number of threads would be equal to the number of cores. The improvement shows that *Sextractor* does not take advantage from all the cores in the machine in which it is run when analysing a single image and the multi-threading implementation of SPADE creates a very positive speed-up.

Table 3.3: Average time needed in seconds for the source detection process to complete. Values for one image and for the entire data-set (86 images) given by the PT-MoD are shown for 1 to 10 threads with both the old and upgraded version. Calculations were performed in a virtual machine with 10GB of RAM and 8 cores and using a 3σ threshold.

Version	Nº of images	Time for different nº of threads (s)				
		1	2	4	8	10
Old	1	0.675	1.087	1.534	2.289	3.294
	86	58.411	46.759	33.138	24.934	28.934
Upgraded	1	0.509	0.552	0.672	0.981	1.256
	86	43.815	23.715	14.668	10.823	11.055

3.6.2 Plate Solving

The second and maybe the most important step in time analysis is plate solving. This step is the one we gave the most attention to as it has the ability to clog the pipeline if it gets stuck on trying to find an astrometric solution.

To avoid this problem we define a maximum time for the process which can be set in the configuration file. The default value chosen is 10 seconds thought to be a tolerable time for special cases to still ensure real-time analysis. This creates a security measure but does not really tackle the problem. In the case that an image surpassed this value, this would mean that a given set of images would not analysed leading to the loss of information and useful night time.

In table 3.4 we can see the time taken for this step without major changes in *Astrometry.net* for each image as well as for all 86 images provided by the PT-MoD with the different number of threads used in multi-threading. As is visible, in 3 out of the 5 multi-thread options there is at least one case where the time is bigger than the time threshold set before. This would mean that SPADE would not analyse these sets.

Table 3.4: Average time in seconds for the standard plate solving process for the set of 86 images given by the PT-MoD, for different number of threads used in multi-threading. Calculations were performed in a virtual machine with 10GB of RAM and 8 cores and using a 3σ threshold.

Number of Threads	1	2	4	8	10
Average Time per image (s)	2.113	2.003	1.811	2.15	3.29
Maximum Time per image (s)	12.811	11.948	8.487	9.946	14.167
Time for 86 images (s)	183.788	85.977	39.016	20.312	28.745

To solve this problem, we decided to reduce the number of detections used. In this new approach we used only the highest SNR detections excluding saturated stars. This parameter was chosen to ensure that we had the sources with the best position precision. This great reduction in the number of detections speeds up *Astrometry.net* leading to a decrease in the step errors. The number of detections may be easily controlled but care is needed in this decision. A smaller number will lead to smaller times but it is possible that the number is too small for *Astrometry.net* to find a solution. In SPADE we saw that there were no errors with 300 sources per image when analysing the entire data-set. Seeing that this step was not one of the slowest in the pipeline and was one of the most important we decided on a default number of 500 sources per image. This was done to make it more resilient to possible special cases in the future that we are not anticipating. We again calculated the time taken to complete this step for the various levels of multi-threading and the results are presented in 3.5.

Comparing tables 3.4 and 3.5 we can see that the selection of sources has a very positive effect on all three analysed times. This is especially true in the maximum times observed per image, where it had a decrease by a factor or 6 in the 8 threads case and there were no case that surpassed the time threshold. This decrease severely diminishes the risk of clogging the pipeline. The same effect that was previously discussed due to multi-threading happens: the time needed

for a particular image increases but the time for the entire data-set decreases as we increase the number of threads. The best case is once again the 8 threads case with an improvement of almost 6 times when compared with the no multi-threading option. This result is very important for real-time analysis applications such as ours.

One last aspect to note is that with this correction, the user can choose to decrease the detection threshold used in section 3.1. We kept the same value of 3σ in SPADE to avoid false positives in other steps but it enables other applications.

Table 3.5: Average time in seconds for the improved plate solving process with only the selected sources for the set of 86 images given by the PT-MoD, for different number of threads used in multi-threading. Calculations were performed in a virtual machine with 10GB of RAM and 8 cores, using a 3σ threshold and 500 selected sources.

Number of Threads	1	2	4	8	10
Average Time per image (s)	0.533	0.574	0.711	0.890	1.777
Maximum Time per image (s)	0.668	0.751	1.390	1.597	3.47
Time for 86 images (s)	46.371	30.783	17.521	7.921	12.143

3.6.3 Photometry

The PSF-fitting photometry process is one of the most time-consuming steps in this pipeline. Two factors may have a strong influence over the time taken by this step: the value of VIGNET used and the number of detections. The reasons are fairly obvious. With a smaller VIGNET SPADE would need to analyse a smaller number of pixels and if we decrease the number of detections, we decrease the number of calculations that are made.

Firstly, the VIGNET parameter. This value can not be decreased without a second thought as it impacts the quality of the fit. It should be big enough to encompass the entire PSF which is on average 6 pixels in the data-set tested. For this reason, we decided that a 15 pixel value would be the minimum value to make sure that the entire PSF was analysed. The maximum value was decided to be 45 pixels, as after that value there would be a lot of interference from nearby sources. The average time per image for 8 threads used in multi-threading can be seen in table 3.6. From this table we can confirm that this parameter influences the step time as the time needed for an image increases significantly. This increase is around 8 times when VIGNET values changes from 15 to 45. This confirms that the user should not just pick a high number as that would lead to significantly more time needed. A balance should be found. In this case SPADE will start to operate with a default value of 15 but it can easily be changed by the user. This value might change in the future when better tests are made to *PSFEx* with the images from the double telescope.

Table 3.6: Average time in seconds for the PSF-fitting process for the 86 images data-set given by the PT-MoD, for different values of VIGNET. Calculations were performed in a virtual machine with 10GB of RAM and 8 cores and using a 3σ threshold.

VIGNET value	15	25	35	45
Time per image (s)	2.393	6.228	11.466	18.528

Secondly, the number of sources. The first question that need answering is how we will select the sources for this step. In figure 3.9 (in page 29) we observed that the sources with positions closest to their respective catalogue matches originated a smaller dispersion. This is expected as well behaved sources will create better photometry values which translates into better source astrometry. For this reason, we decided to use this as the parameter to reduce the number of sources. This number can be controlled in the configuration file. We decided on selecting 200 sources for testing, with the results shown in table 3.7. As we could not be absolute certain of the

quality of the fit with this data-set we increased the VIGNET to 25 for the following analysis, to not leave any doubt.

This table shows that the number of sources does not actually have a big impact on the time contrary to the expected. This is because *PSFEx* already has a built-in system to only choose the best sources and for the images provided by the PT-MoD this is already a small number. The maximum decrease observed is only of 0.3 seconds, not significant. More testing should be done with other set of images to understand if this is still the case or if we can improve with this option.

Table 3.7: Average time in seconds for the PSF-fitting process for the 86 images data-set given by the PT-MoD, for different number of sources used and VIGNET=25. Calculations were performed in a virtual machine with 10GB of RAM and 8 cores.

Number of Sources	50	100	200	300	400	500
Time per image (s)	5.716	5.869	5.912	6.086	5.991	6.066

In table 3.8 the multi-threading effect on this step is shown. We can observe that the time taken per image does not increase significantly. This suggests that PSFEx, even though it is a recent software, does not take full advantage of multi-threading. This originates a decrease of around 7 times for the 8 threads case. This creates another case of great success for the multi-threading of SPADE, greatly speeding up the process.

Table 3.8: Average time in seconds for the PSF-fitting process for the 86 images data-set given by the PT-MoD, for different number of threads used in multi-threading with VIGNET=25 and 200 sources used. Calculations were performed in a virtual machine with 10GB of RAM and 8 cores.

Number of Threads	1	2	4	8	10
Time per image (s)	5.363	5.271	5.625	5.912	7.038
Time for 86 images (s)	462.941	229.034	122.491	64.202	62.518

3.6.4 Catalogue Comparison

In the catalogue comparison step two hypotheses were tested: either reading the catalogue at the beginning or reading only the portion of the catalogue that would be visible for each image. The advantage of the first method is that it would be much faster as it would only require SPADE to read the catalogue once and could be done before the image acquisition even began. Reading it for each image, even if in smaller chunks, would put an additional strain on SPADE. The disadvantage is that a much larger catalogue needs to be kept in memory permanently. In practice, in a single night of observations we are not preoccupied with the entire sky. This means that we do not even need to read the entire catalogue, only the portion that we are expected to observe. For this reason SPADE asks for the minimum and maximum declination that will be observed in that night and only reads that portion of the sky. When we introduce multi-threading, this problem complicates. In the second option we will have to load multiple catalogue chunks simultaneously and possibly leading to more RAM usage. To decide which option would be best, the performance of both options were tested. The time taken and the RAM consumed were measured and shown in tables 3.9 and 3.10. One aspect that needs to be noted is that the catalogue was only read up to magnitude 16. This is because the faintest sources in the data-set had magnitudes just over 15. This is true for the PT-MoD but may vary with our setup and even throughout the year. This magnitude limit can be controlled in the configuration file and the decision is up to the operator. In PASO this decision will be made when the double telescope setup becomes operational.

It is immediately visible that the first method of reading the catalogue right at the start is by far the fastest. For the case of 8 threads used in multi-threading time the improvement is of a factor of 61. Not only that, the time needed for the second option far surpasses the previous steps and would be impossible to ensure real-time analysis.

Table 3.9: Average time in seconds for the catalogue comparison process when reading at the beginning of SPADE for the 86 images data-set given by the PT-MoD, for different number of threads used in multi-threading. There is also available the total time required by SPADE to process the entire set of images. Calculations were performed in a virtual machine with 10GB of RAM and 8 cores, the catalogue read up to magnitude 16 and using a 3σ threshold.

Number of Threads	1	2	4	8	10
Time per image (s)	0.506	0.527	0.635	0.793	1.143
Time for 86 images (s)	43.624	22.767	13.998	8.809	10.299
RAM (GB)	2.05	2.15	2.35	2.99	3.24

Table 3.10: Average time in seconds for the catalogue comparison process when reading for every image for the 86 images data-set given by the PT-MoD, for different number of threads used in multi-threading. There is also available the total time required by SPADE to process the entire set of images. Calculations were performed in a virtual machine with 10GB of RAM and 8 cores and the catalogue read up to magnitude 16 and using a 3σ threshold.

Number of threads	1	2	4	8	10
Time per image (s)	5.276	11.648	23.496	49.137	62.182
Time for 86 images (s)	453.921	444.326	499.134	542.010	548.009
RAM (GB)	1.36	1.38	1.53	1.93	2.04

When looking at RAM, we confirm that the first method consumes more memory even for higher number of threads used. But this increase is not significant enough to compensate for the huge decrease in computational speed. These values confirm that SPADE should use the method of reading the catalogue in the beginning instead of small chunks in between. If the magnitude limit increases significantly (ex: up to magnitude 19) the RAM used will follow suit. This is not expected as we will mainly use low exposure times like the ones seen in this data-set and our optical setup magnitude limit is similar to the PT-MoD telescope. If special circumstances force the usage of these magnitudes, the better option would still be to simply to upgrade the RAM available to the system over decreasing the number of threads.

The second method will only be useful if by any chance, the telescope moves outside the initially defined range, no catalogue information will be available. In those special cases, SPADE will perform the second method, reading only the part which is relevant to the image in question.

3.6.5 Image Cross-Referencing

The detection of debris is only done once for each set of 4 images, so the time tolerated for each individual image in this step is bigger than in the previous ones which are applied to every single image. It is harder to gauge the performance of this step as we need to measure the time and the number of false positives and false negatives. As has already been discussed, for SST purposes the presence of false positives is very damaging to the data which means that SPADE prefers to tolerate some false negatives. The dominant factor to the time needed for this step is the number of detections in an image, which is dependent on the threshold used in the source detection step. In table 3.11 we present the times taken for this step for different values of threshold used. Only the 60 images that were grouped in sets of 4 were used in this process, as the data-set of 26 images is not organized in sets of 4 and is not suited fro this test.

As is immediately visible, the time needed for cross-referencing increases exponentially when using lower thresholds. Both 3σ and 5σ thresholds originate a average time small enough to be used for real-time analysis. When using 2σ the time taken is too big for SST purposes. A time of over 20 seconds per set, which happens in this data-set, means an average of 5 seconds per image. This would possibly clog the pipeline. This is another reason to favor 3σ over 2σ threshold.

Table 3.11: Average time in seconds for the image cross-referencing process for the data-set of 60 images from the PT-MoD, for 8 threads used in multi-threading. There is also available the total time required by SPADE to process the entire set of images. Calculations were performed in a virtual machine with 10GB of RAM and 8 cores.

Cross-Referencing limit	Average Time (s)	Average nº of Detections	Minimum Time (s)	Maximum Time (s)
2σ	9.600	3536	2.718	21.364
3σ	0.669	1978	0.363	1.972
5σ	0.428	1246	0.261	1.04

3.6.6 Satellite Identification

To understand which satellites are visible in our images, SPADE needs to check every single TLE available in the data-set for each set of images observed. This proves to be a hard task for the system as can be observed in table 3.12. Only the 60 images that were grouped in sets of 4 were used in this process as the data-set of 26 images is not in a zone of interest for the GEO and MEO region.

The time taken for this step completely dominates all previous step, with the smallest time being just over 2 minutes for the 1 thread case. Unlike previous steps, the time taken does not decrease with the use of multi-threading with the best case actually being 1 thread but with comparable numbers with all the other cases. This step is only an option for SPADE so it is not as worrying but these values show that this part of SPADE can be improved upon to better optimize the search in order to greatly decrease the overall time if this option is required.

Table 3.12: Average time in seconds for the satellite identification step for the data-set of 60 images given by the PT-MoD, for different number of threads used in multi-threading. There is also available the total time required by SPADE to process the entire set of images. Calculations were performed in a virtual machine with 10GB of RAM and 8 cores.

Number of Threads	1	2	4	8	10
Time per image (s)	7.895	19.505	33.338	74.146	88.013
Time for 60 images (s)	121.864	146.605	126.119	141.923	134.815

3.6.7 Full Pipeline

The time taken for the full pipeline is of vital importance for SPADE as it determines the number of images we can analyse in real time as well as the hardware requirements for future improvements. We want to make sure that each image begins to be analysed by SPADE, without the need of queueing behind active processes. The PT-MoD telescope has the same sensor and similar FoV leading to comparable pixel scale (4.6) when compared with our double telescopes (4.04) when binned. For this reason for the following discussion we assume that our future operation will be similar to the PT-MoD's, with a 5 second interval between image. In our case, this will be 2 images every 5 seconds, one for each telescope.

Seeing that the Satellite Identification process and the cosmic ray removal dominate the time taken for the pipeline and is an optional task, we chose to analyse the pipeline with and without these step. With these values we can calculate what would be the optimal number of threads to use taking into account both the time taken to process the images and the expected number of images that SPADE is expected to be analysing at a given time. These values can be seen in table 3.13.

If we assume that there is no movement between images, the time needed to take all 60 images with a 5 second interval will be 300 seconds for the PT-MoD and 150 seconds for our double telescopes.

If we look at the case where both satellite identification and cosmic ray removal are made, no multi-threading option would be enough for both cases. The best case would be using 10 thread according to the information, which would require 2 similar processors as the one used to test for the PT-MoD image acquisition times and 4 for our case. This does not originate a large problem though, as satellite identification is a special service that is not required by the SST. These calculations are made in an operational center after the positional data is provided by SPADE. For that reason, this will not be the normal function of SPADE in the future. This step was used as a verification step during the development, but is an additional step already available for SPADE if a client requires it in the future, and can be enabled in the configuration file if needed.

If we look at the case without satellite identification but with cosmic rays, which is the one we will use in the beggining of the double telescope operation, it is capable of analysing the PT-MoD with 4, 8 or 10 threads but no option fits our case. In our case we would need two similar processors, one for each telescope. A better processor with more cores could also be tested. Looking at the time values the 4 thread case would produce the results faster for each image, but overall time would be slower which is the more important factor. Slower overall times will decrease the chance of clogging the pipeline. For this reason, this would be the best option. When the double telescope becomes fully operational we will use the number of threads equal to the number of cores that we implement. These results show that SPADE is capable of processing telescope images in real-time to detect RSOs.

If we look at the time needed with neither satellite identification nor cosmic ray reduction, even the no multi-threading option works for the PT-MoD. For our case multi-threading is needed, with all other cases working. These results show that even if the future operations special cases require a time interval smaller than the 5 seconds predicted, we can remove the cosmic ray to guarantee real-time analysis. Due to the possible cons of removing this step we propose the acquirement of 2 processors to be capable of executing a complete image reduction. In the case of the PT-MoD SPADE could be used without further investment, as it is a single telescope.

Table 3.13: Average time in seconds for the entire SPADE pipeline for all 15 sets of images given by the PT-MoD, for different number of threads used in multi-threading. There is available both the time with or without satellite identification, both without PSF-fitting photometry. Calculations were performed in a virtual machine with 10GB of RAM and 8 cores and using a 3σ threshold. CR - Cosmic Ray

	Number of Threads	1	2	4	8	10
With Satellite Identification	Time per image (s)	11.709	20.433	38.966	71.645	79.568
	Time for 60 images (s)	702.537	628.443	600.022	610.808	570.437
Without Satellite Identification	Time per image (s)	7.478	10.747	19.056	37.162	46.548
	Time for 60 images (s)	452.121	324.941	287.562	279.948	283.481
Without Satellite Identification and CR correction	Time per image (s)	3.204	3.681	6.314	11.957	14.757
	Time for 60 images (s)	194.502	112.58	96.182	91.104	92.991

Chapter 4

Conclusion

This thesis had the goal to create, from scratch, a RSO detection pipeline to analyse in real-time the images from the new double telescope in PASO. This task was concluded with success with the creation of SPADE. It is capable of performing astrometry with the 2 arcsec precision needed for the SST. This was tested with a star catalogue comparison and will be verified when the entire system passes through a calibration test with the SST. SPADE consists of three main parts: reduction, source detection and characterization, RSO identification and classification. SPADE has extra tools available such as PSF-fitting photometry and satellite identification from available TLEs. These are not required by the SST but can be used with SPADE. Without the reduction process, the pipeline can be run on the personal computer used to develop the code. In the case where reduction is performed, two similar processors are required to guarantee real-time analysis without clogging. The system was tested with images from the PT-MoD with focus and collimation problems as well as source duplication possibly due to strong winds. Still SPADE was capable of extracting good information from them. We could not test *PSFEx* with the given images, but will be done with future images.

In the reduction process SPADE applies the most common dark and flat-field corrections as well as corrections for crosstalk, cosmic rays, gain and background. Every individual step can be enabled or disabled in the configuration file separately in accordance with the user preference. By analysing the time taken for each step we concluded that the most computational intensive step was cosmic ray correction. This step dominates the time required for this process, surpassing the second slowest (background removal) by a factor of 10. In case SPADE needs to operate faster, this is the first correction which will be removed even though it is considered the most important as all other steps don't have a significant effect. We also concluded that the dark and flat-field corrections did not have a significant impact in the time taken for the pipeline while creating good improvements. For this reason this correction will be used in PASO. All information is written in the header of the file to facilitate further analysis.

In the source detection and characterization part, the pipeline makes use of *Sextractor* and *Astrometry.net* for source detection and plate solving respectfully. The default value for detection threshold used in SPADE is 3σ but it can be easily changed to match a specific purpose. This choice was made because in cases where lower threshold values are used the number of detections increases significantly which in term increases the computational time and originates false positives that we want to avoid. The quality of the plate-solving was tested with a catalogue comparison. We decided to use the UCAC5 catalogue for star matching and for future photometry. This decision was made principally for the quality of the astrometry in this catalogue which is in the miliarcseconds, much smaller than the limit of our equipment. In this test we found that 65.9% of sources were closer than the 2 arcsec requirement with a median value of 1.45 arcsec. Even though it is not yet a EU-SST requirement, photometry of sources is also implemented with the use of *Sextractor* with a isophotal method or *PSFEx* with the more accurate but more costly PSF matching. This tool was created in preparation for planned future SPADE applications for and to easily react to updates of EU-SST requirements. To speed up the pipeline, in each step in which

it is possible SPADE selects the only the best detections. This selection can easily be controlled in the configuration file. SPADE only reads a portion of the sky chosen by the user in order to reduce the burden on the machine which helps to reduce the investment needed.

Debris classification from detected sources is done by one of two methods: catalogue comparison or image cross-referencing. The preferred method used in SPADE is the latter, which not only involves a smaller computational cost but also produces significantly less false positives, a determinant factor in this application. The first method will only be used if in the off chance that only a single image from a field is available. After classification of a debris/satellite, SPADE also has the option to search for an object match with in the Celestrak TLE catalogue. This step will be usually performed in a latter stage by the EU-SST but its already an option if a future client requires it. In the data-set given by the PT-MoD SPADE detected 7 out of the 21 TLE expected RSO. The expected RSO was not visible in 7 cases, in one case it was on the border and in other 2 cases it was on top of a star. Removing these special cases SPADE works in 7 out of 11 cases (63.6%) which is promising.

Although further improvement and features will continuously be added to SPADE throughout its lifetime, it is already considered a product and is able to process data in real-time without human intervention. The pipeline is capable of analysing objects in GEO and slower MEO orbits. LEO objects will be tested when the telescope in PASO starts operating in such conditions. One of the biggest advantages of the pipeline is that it was designed such that it can be easily personalized to fit various optical systems. The future operations in PASO will also involve science imaging. SPADE was also created in order to work in both cases, not requiring the creation of another tool. Every step from the pipeline can be easily controlled by only tuning the configuration file in accordance with the equipment used and the objective of the user without the need to change any of the code or understanding in depth all of its inner workings. Every action performed is logged to facilitate analysis in the case of an error occurring during normal operations, greatly decreasing the time needed to fix small problem that may occur.

Future work to improve the present tools in SPADE will involve the use of multivariate statistics to determine what parameters better differentiate satellites/debris from stars in our images. This could not only significantly speed up our pipeline due to the decrease in computational cost per image but could also reduce the number of images we have to take per field. In addition, a tool to take advantage of the already built photometry ability of SPADE is being developed to analyse satellite light curves and sky position to obtain different orbital parameters which can improve future predictions. In the future, the pipeline will also be complemented with a line detection tool to analyse LEO orbits.

Appendix A

SPADE folder chart

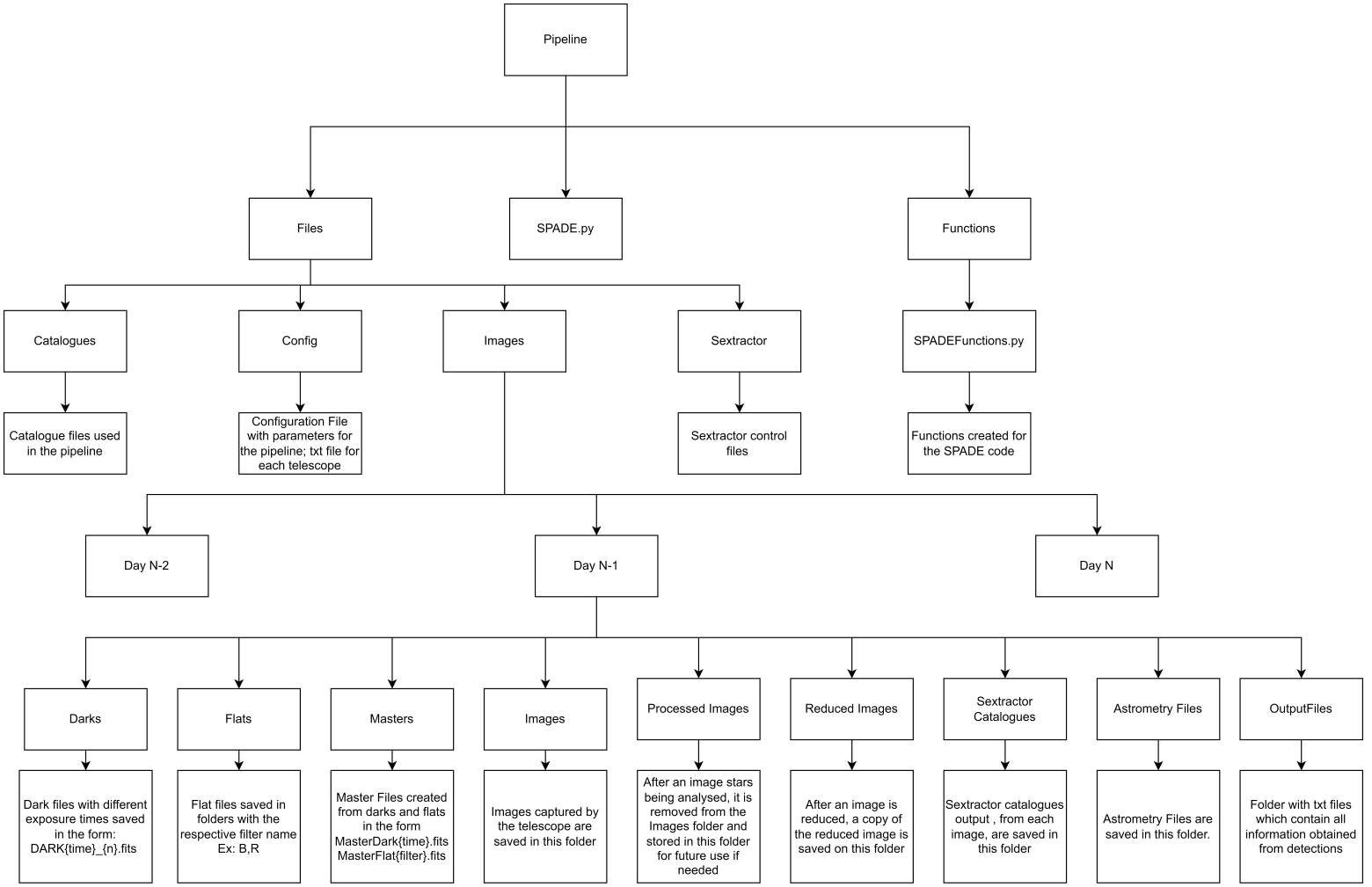

Figure A.1: SPADE folders chart including their descriptions.

References

Abbott, T. M. C., Adamów, M., Aguena, M., Allam, S., Amon, A., Annis, J., Avila, S., Bacon, D., Banerji, M., Bechtol, K., Becker, M. R., Bernstein, G. M., Bertin, E., Bhargava, S., Bridle, S. L., Brooks, D., Burke, D. L., Rosell, A. C., Kind, M. C., ... Server), (S. (2021). The dark energy survey data release 2. *The Astrophysical Journal Supplement Series*, *255*(2), 20. https://doi.org/10.3847/1538-4365/ac00b3

Annunziatella, M., Mercurio, A., Brescia, M., Cavuoti, S., & Longo, G. (2013). Inside catalogs: A comparison of source extraction software. *Publications of the Astronomical Society of the Pacific*, *125*, 68–82. https://doi.org/10.1086/669333

Bertin, E., & Arnouts, S. (1996). SExtractor: Software for source extraction. *aaps*, *117*, 393–404. https://doi.org/10.1051/aas:1996164

Bertin, E. (2013). Psfex: Point spread function extractor. *Astrophysics Source Code Library*.

Cegarra Polo, M., Yanagisawa, T., & Kurosaki, H. (2022). Real-time Processing Pipeline for Automatic Detection and Identification of Faint Streaks in Astronomical Images through multi-CPU/GPU Heterogeneous Computing. *44th COSPAR Scientific Assembly. Held 16-24 July*, *44*, 3147.

Coelho, B. Developing a data fusion concept for radar and optical ground based sst station. (IAC, Ed.). In: ed. by IAC. *73*. 2022, September. http://hdl.handle.net/10400.21/15981

ESA. (2022). Esa's space environment report 2022. https://www.esa.int/Space_Safety/Space_Debris/ESA_s_Space_Environment_Report_2022

European Comission. (2022, July). Commission implementing decision (eu) 2022/1245. https://eur-lex.europa.eu/legal-content/EN/TXT/PDF/?uri=CELEX:32022D1245

Evans, M. S. (2010). Achieving continuity: A story of stellar magnitude. *Studies in History and Philosophy of Science Part A*, *41*(1), 86–94. https://doi.org/https://doi.org/10.1016/j.shpsa.2009.12.007

Gasdia, F. (2016). *Optical tracking and spectral characterization of cubesats for operational missions* [Master's Thesis]. Embry-Riddle Scholarly Commons.

Gasdia, F., Barjatya, A., & Bilardi, S. (2017). Multi-site simultaneous time-resolved photometry with a low cost electro-optics system. *Sensors*, *17*, 1239. https://doi.org/10.3390/s17061239

Gavras, P., Rimoldini, L., Nienartowicz, K., de Fombelle, G. J., Holl, B., Ábrahám, P., Audard, M., Carnerero, M., Clementini, G., De Ridder, J., Distefano, E., Garcia-Lario, P., Garofalo, A., Kóspál, Á., Kruszyńska, K., Kun, M., Lecoeur-Taïbi, I., Marton, G., Mazeh, T., ... Eyer, L. (2022). Gaia data release 3: Cross-match of gaia sources with variable objects from the literature. https://doi.org/10.48550/ARXIV.2207.01946

Gonçalves, L. Clown: A new tool for cloud detection with all-sky camera for optimization of space-debris surveys. (IAC, Ed.). In: ed. by IAC. *73*. 2022, September. https://www.eusst.eu/wp-content/uploads/2022/11/IAC-22_CLOWN.pdf

Gonçalves L., B., Coelho, D., Barbosa, M., Bergano, V., & Bonifácio. (2023). Clown: The paso cloud detection for optimization of automatic optical surveys [in prep.].

Høg, E., Fabricius, C., Makarov, V. V., Urban, S., Corbin, T., Wycoff, G., Bastian, U., Schwekendiek, P., & Wicenec, A. (2000). The Tycho-2 catalogue of the 2.5 million brightest stars. *aap*, *355*, L27–L30.

Holwerda, B. W. (2005). Source extractor for dummies v5. https://arxiv.org/abs/astro-ph/0512139

Jordan, J., Posada, D., Gillette, M., Zuehlke, D., & Henderson, T. (2023). Quasi real-time autonomous satellite detection and orbit estimation. https://www.researchgate.net/publication/370001014_Quasi_Real-Time_Autonomous_Satellite_Detection_and_Orbit_Estimation

Jordan, J., Posada, D., Zuehlke, D., Radulovic, A., Malik, A., & Henderson, T. (2022). Satellite detection in unresolved space imagery for space domain awareness using neural networks. https://www.researchgate.net/publication/362252394_Satellite_Detection_in_Unresolved_Space_Imagery_for_Space_Domain_Awareness_Using_Neural_Networks

Kessler, D. J., & Cour-Palais, B. G. (1978). Collision frequency of artificial satellites: The creation of a debris belt. *Journal of Geophysical Research*, *83*, 2637–2646.

Lang, D., Hogg, D. W., Mierle, K., Blanton, M., & Roweis, S. (2010). Astrometry.net: Blind Astrometric Calibration of Arbitrary Astronomical Images. *aj*, *139*(5), 1782–1800. https://doi.org/10.1088/0004-6256/139/5/1782

Mark Rigby, B. C. (2021). A chunk of chinese satellite almost hit the international space station. they dodged it – but the space junk problem is getting worse. https://theconversation.com/a-chunk-of-chinese-satellite-almost-hit-the-international-space-station-they-dodged-it-but-the-space-junk-problem-is-getting-worse-171735

McCullough, P. (2008, August). Inter-pixel capacitance: prospects for deconvolution. https://ui.adsabs.harvard.edu/abs/2008wfc..rept...26M/abstract

McCully, C., Crawford, S., Kovacs, G., Tollerud, E., Betts, E., Bradley, L., Craig, M., Turner, J., Streicher, O., Sipocz, B., Robitaille, T., & Deil, C. (2018, November). *Astropy/astroscrappy: V1.0.5 zenodo release* (Version v1.0.5). Zenodo. https://doi.org/10.5281/zenodo.1482019

Pandeirada, J., Bergano, M., Neves, J., Marques, P., Barbosa, D., Coelho, B., & Ribeiro, V. (2021). Development of the first portuguese radar tracking sensor for space debris. *Signals*, *2*(1), 122–137. https://www.mdpi.com/2624-6120/2/1/11

Paterson, K. (2017). Meerlicht: Meerkat's optical eye. *Proceedings of the International Astronomical Union*, *14*, 203–203. https://doi.org/10.1017/S1743921318002594

Patterson, K. (2018). *Detecting optical transients and variables with meerlicht* [Doctoral dissertation]. UCT. http://hdl.handle.net/11427/29987

Perryman, M. A. C., Lindegren, L., Kovalevsky, J., Hog, E., Bastian, U., Bernacca, P. L., Creze, M., Donati, F., Grenon, M., Grewing, M., van Leeuwen, F., van der Marel, H., Mignard, F., Murray, C. A., Le Poole, R. S., Schrijver, H., Turon, C., Arenou, F., Froeschle, M., & Petersen, C. S. (1997). The Hipparcos Catalogue. *Astronomy and Astrophysics*, *500*, 501–504.

Piergentili, F., Zarcone, G., Parisi, L., Mariani, L., Hossein, S. H., & Santoni, F. (2021). Leo object's light-curve acquisition system and their inversion for attitude reconstruction. *Aerospace*, *8*(1). https://doi.org/10.3390/aerospace8010004

Rhodes, B. (2019, July). Skyfield: High precision research-grade positions for planets and Earth satellites generator.

Schlafly, E. F., Green, G. M., Lang, D., Daylan, T., Finkbeiner, D. P., Lee, A., Meisner, A. M., Schlegel, D., & Valdes, F. (2018). The decam plane survey: Optical photometry of two billion objects in the southern galactic plane. *The Astrophysical Journal Supplement Series*, *234*(2), 39. https://doi.org/10.3847/1538-4365/aaa3e2

Sheetz, M. (2022). U.s. commits to ending anti-satellite missile testing, calls for global agreement. https://www.cnbc.com/2022/04/18/us-to-end-anti-satellite-asat-testing-calls-for-global-agreement.html

Silha, J., Schildknecht, T., Hinze, A., Utzmann, J., Wagner, A., Willemsen, P., Teston, F., & Flohrer, T. (2014). Capability of a space-based space surveillance system to detect and track objects in geo, meo and leo orbits. *2*, 1160–1167.

Stetson, P. B. (1987). Daophot: A computer program for crowded-field stellar photometry. *Publications of the Astronomical Society of the Pacific*, *99*(613), 191. https://doi.org/10.1086/131977

Subramaniam, V. (2011). *Programming concurrency on the JVM : Mastering synchronization, STM, and actors*. Pragmatic Bookshelf. http : / / www . amazon . com / Programming - Concurrency - JVM - Mastering - Synchronization / dp / 193435676X / ref = sr _1 _1 ? ie = UTF8 % 5C & qid = 1366807930 % 5C & sr = 8 - 1 % 5C & keywords = programming + concurrency + on + the + jvm

Sun, R.-y., Zhan, J.-w., Zhao, C.-y., & Zhang, X.-x. (2015). Algorithms and applications for detecting faint space debris in geo [Dynamics and Control of Space Systems]. *Acta Astronautica*, *110*, 9–17. https://doi.org/https://doi.org/10.1016/j.actaastro.2015.01.001

Tawalbeh, Y., & Al-Wardat, M. (2018, May). *Modified orbital elements of the close visual binary systems hip11352, hip70973, and hip72479* [Doctoral dissertation, Al al-Bayt University].

Vallado, D., & Cefola, P. (2012). Two-line element sets - practice and use. *Proceedings of the International Astronautical Congress, IAC*, *7*, 5812–5825.

Virtanen, J., Poikonen, J., Säntti, T., Komulainen, T., Torppa, J., Granvik, M., Muinonen, K., Pentikäinen, H., Martikainen, J., Näränen, J., Lehti, J., & Flohrer, T. (2016). Streak detection and analysis pipeline for space-debris optical images. *Advances in Space Research*, *57*, 1607. https://doi.org/10.1016/j.asr.2015.09.024

Vision, M., & Robotics. (2020). What are the benefits of cmos based machine vision cameras vs ccd? http://www.mvrpl.com/Industrial-Machine-Vision-Cameras-dealer-in-Mumbai-India-What-are-the-benefits-of-CMOS-based-machine-vision-cameras-vs-CCD-Jan-2020.html

Zhao, X.-F., Yu, Y., Mao, Y.-D., & Tang, Z.-H. (2021). Long-term photometric signature study of two geo satellites. *Advances in Space Research*, *67*(8), 2241–2251. https://doi.org/https://doi.org/10.1016/j.asr.2021.01.051

Zigo, M., Silha, J., & Krajčovič, S. (2019, September). BVRI Photometry of Space Debris Objects at the Astronomical and Geophysical Observatory in Modra. In S. Ryan (Ed.), *Advanced maui optical and space surveillance technologies conference* (p. 33).

Zuehlke, D., Posada, D., Tiwari, M., & Henderson, T. (2021, February). *(preprint) aas 21-364 autonomous satellite detection and tracking using optical flow.*